

## 5. Structural properties of hyperbranched polymers

### 5.1. Conformation of simulated hyperbranched polymers

In this work, two series of hyperbranched polymers were simulated using the coarse-grained uniform bead model in order to characterize the effect of molecular weight and inter-branch spacing on structural and rheological properties of hyperbranched polymer melts. This model has been successfully used in an NEMD study of dendrimers (Bosko et al., 2004a).

The first series of simulated hyperbranched polymers have molecular weights corresponding to those of tri-functional dendrimers as this allows a comparison between our simulation data and previously reported results for linear polymers and dendrimers (Bosko et al., 2004a, Bosko et al., 2004b, Bosko et al., 2005, Bosko et al., 2006). The total number of beads in dendrimers can be defined as:

$$N_s = fb((f-1)^{g+1} - 1)/(f-2) + 1 \quad (5.1)$$

where  $f$  is the functionality of end groups,  $b$  is the number of monomers in the chain units and  $g$  is the generation number. With the choice of  $f = 3$  and  $b = 2$ , dendrimers of generation 1, 2, 3 and 4 will have 19, 43, 91 and 187 beads respectively. Therefore the hyperbranched polymer chains generated in this work are composed of 19, 43, 91 and 187 interconnected beads. A simple specific architecture of hyperbranched polymers has been chosen. They are dendrimers with trifunctional end groups ( $f = 3$ ) and two beads in the chain units ( $b = 2$ ) that have one imperfect branching point ( $f = 2$ ). As our hyperbranched polymers have the same number of beads as dendrimers but fewer branches at one branching point, extra beads are added in the outer-most layer of the molecules with  $f = 3$  and  $b = 2$ . The schematic configuration of these hyperbranched polymers (type A) is presented in Figure 5.1 and their typical instantaneous configurations in comparison with dendrimers and linear polymers are shown in Figure 5.2.

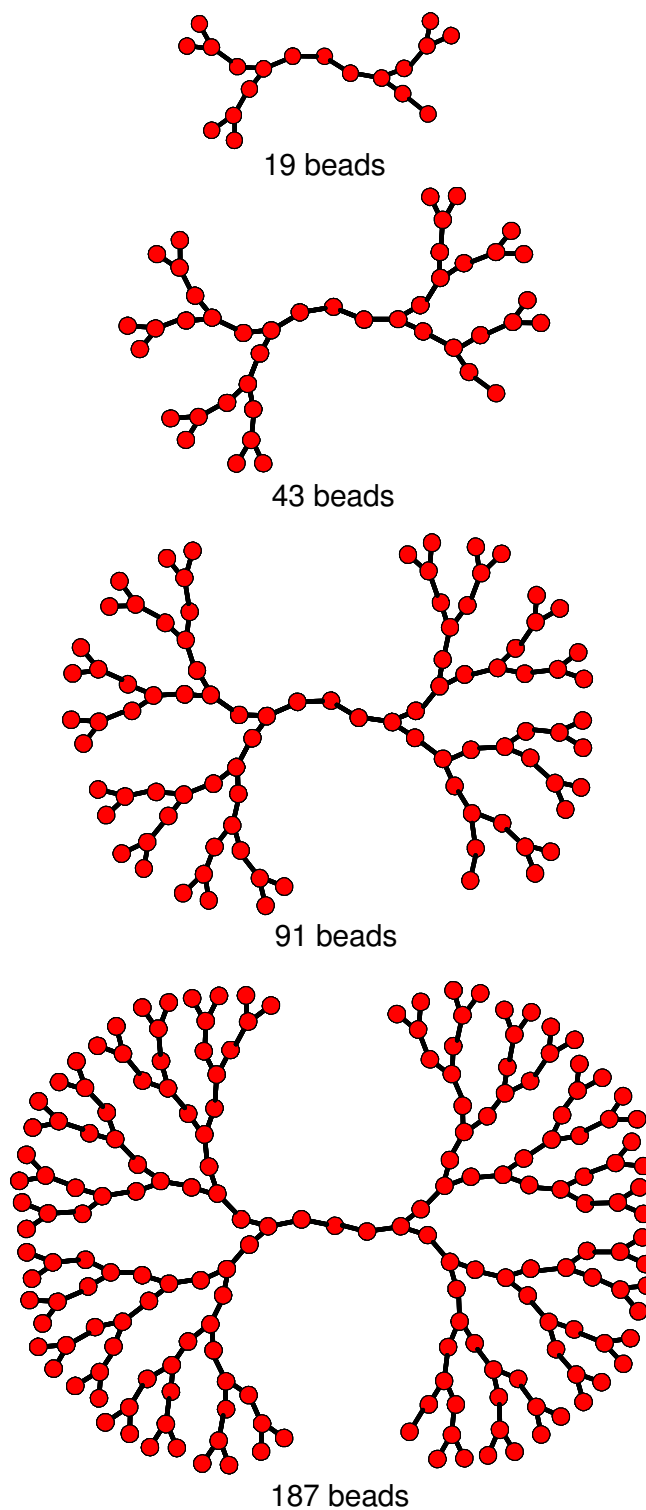


**Figure 5.1.** Schematic architectures of type A hyperbranched polymers of different molecular weights.

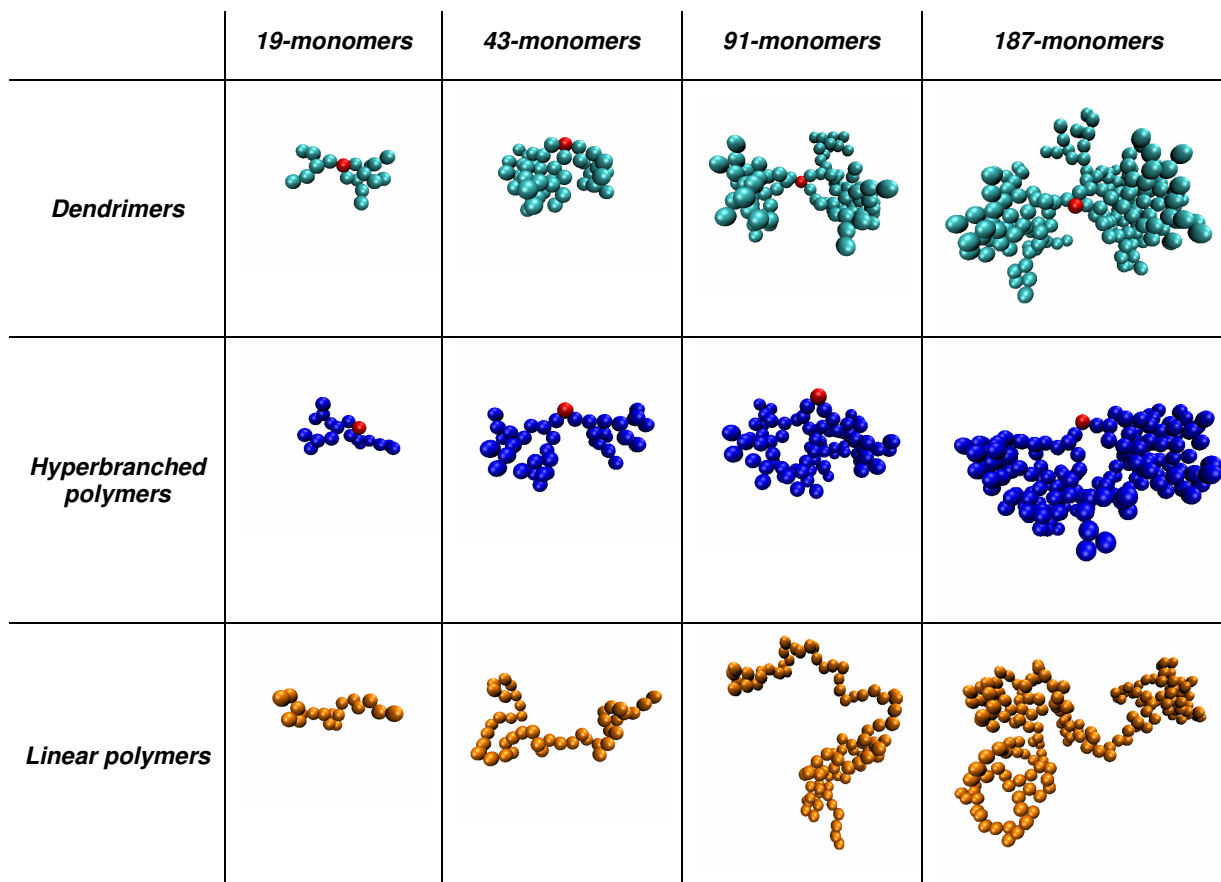


**Figure 5.2. Configuration of type A hyperbranched polymers with different molecular weights in comparison with dendrimers and linear polymers.**

The hyperbranched polymers of the second series have the same molecular weight but different chain lengths between branches. They all have the same degree of polymerization  $N_s$  of 187, as for a perfect dendrimer of generation 4, and one imperfect branching point with the functionality of end groups  $f = 2$ . The only difference in their architectures is the number of spacer units. Hyperbranched polymers of type A as mentioned above have two beads in the chain units ( $b = 2$ ) while polymers of type B, C and D have three, four and five beads, respectively, in the chain units. The schematic configuration of these hyperbranched polymers is presented in Figure 5.3 whereas their typical instantaneous configurations are shown in Figure 5.4.

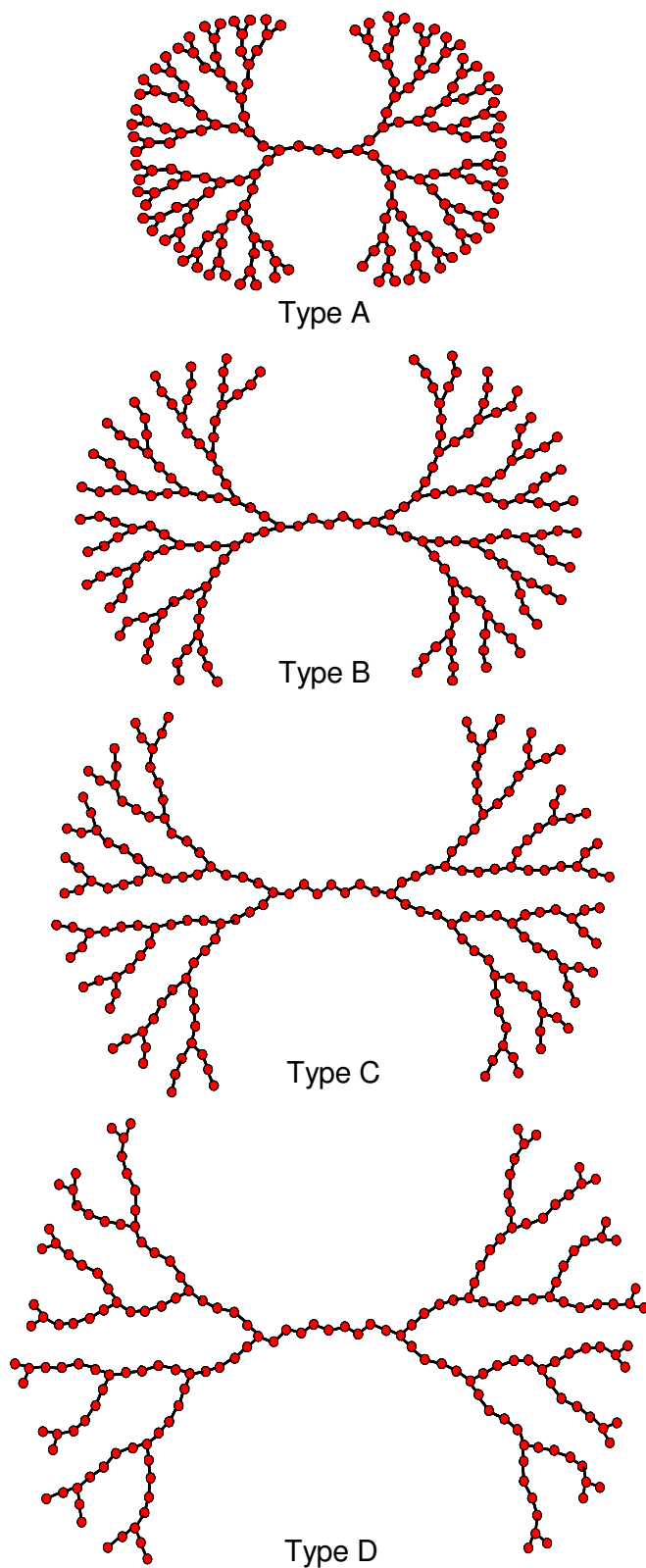
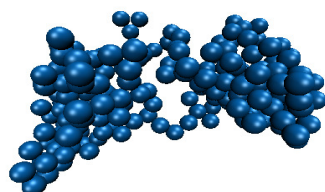
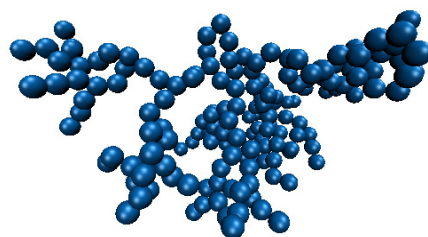


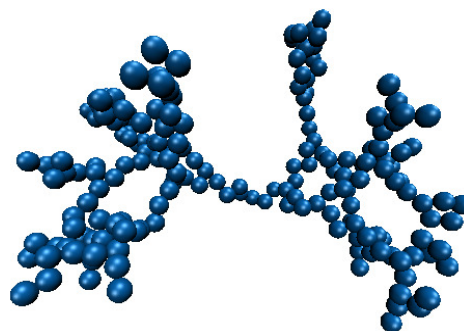
**Figure 5.3.** Schematic architectures of hyperbranched polymers of the same molecular weight of 187 beads but different number of spacers.



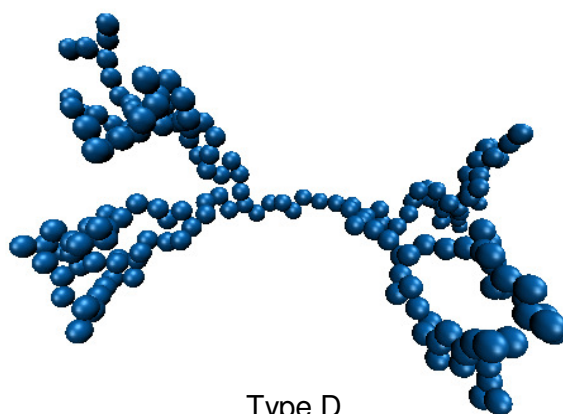
Type A



Type B



Type C



Type D

**Figure 5.4. Configurations of hyperbranched polymers comprising 187 beads but with different number of spacers.**

The structure of hyperbranched polymers of the same molecular weight can normally be characterized by two different structural parameters, the degree of branching and the Wiener index. These values for simulated hyperbranched polymers with different numbers of spacers are shown in Table 5.1.

**Table 5.1. Degree of branching and Wiener index for hyperbranched polymers of the same molecular weight of 187 beads but with different number of spacers.**

Type of hyperbranched polymers	Degree of branching	Wiener index
A	0.9920	123,194
B	0.9920	153,122
C	0.9836	174,986
D	0.9836	193,770

The degree of branching, as previously mentioned, can be calculated as:

$$B = 2D / (2D + L) \quad (5.2)$$

where  $D$  is the number of fully branched beads and  $L$  is the number of partially reacted beads. The value of the degree of branching varies from 0 for linear polymers to 1 for dendrimers or fully branched hyperbranched polymers. As all simulated systems have only one imperfect branching point, the value of  $L$  is always 1. Hyperbranched polymers of type A and B have the same number of fully branched beads of 61 hence they have the same degree of branching of 0.992. Polymers of type C and D have the same number of fully branched beads of 30. Therefore they have the same degree of branching of 0.9836. The same values of the degree of branching for different hyperbranched polymers indicate that this parameter only characterizes the extent of unbranched content within a hyperbranched molecule and does not fully describe the architecture of the systems. This is in agreement with many other reports (Neelov and Adolf, 2004, Sheridan et al., 2002, Lyulin et al., 2001, Widmann and Davies, 1998) on hyperbranched polymers.

In addition to the degree of branching, the Wiener index, defined as:

$$W = \frac{1}{2} \sum_{j=1}^{N_s} \sum_{i=1}^{N_s} d_{ij} \quad (5.3)$$

where  $N_s$  is the number of beads per molecule and  $d_{ij}$  is the number of bonds separating bead  $i$  and  $j$  of the molecule, was calculated to characterize the topologies of simulated hyperbranched polymers in greater detail. This parameter only describes the connectivity and is not a direct measure of the size of the molecules. For polymers of the same molecular weight, the linear chain has the largest value of  $W$  whereas the star polymer with branch length of 1 and the core functionality of  $N_s - 1$  has the smallest value of  $W$ . In this work, the Wiener index is largest for the type D system which has the longest linear chain in between branching points (number of spacers  $b=5$ ) and smallest for the type A system which has the shortest linear chain between branching points ( $b=2$ ). With increasing number of spacers from 2 to 5, the values of the Wiener index for hyperbranched polymers comprising 187 beads increase and fall in the range between 123,194 and 193,770. Polymer systems with higher number of spacers or higher Wiener index have more open structure and larger topological separation of beads.

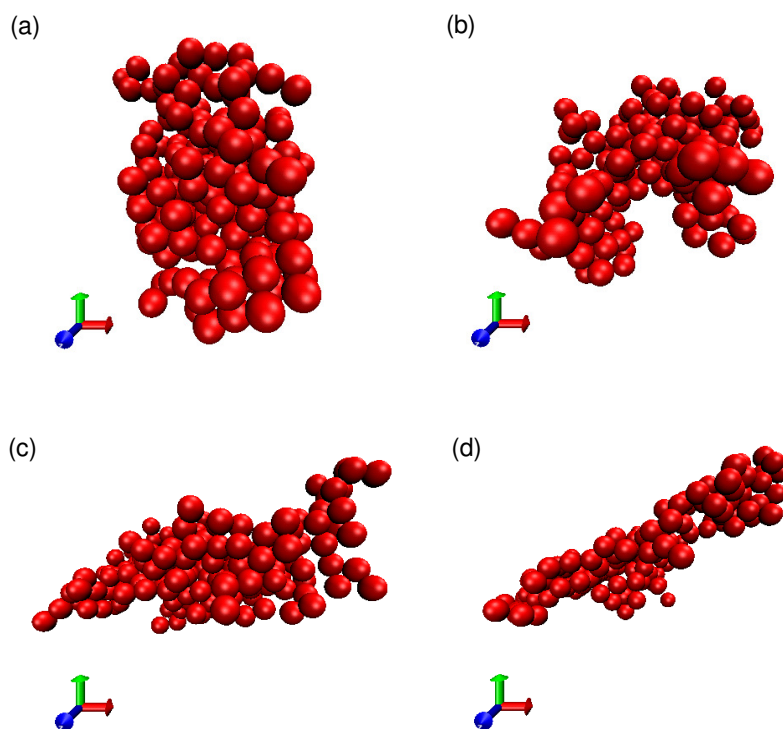


**Figure 5.5. Configuration of type A hyperbranched polymer with 187 monomers at strain rates of (a) 0.0001, (b) 0.001, (c) 0.01 and (d) 0.1.**

In contrast to all previous studies which addressed the simulation of hyperbranched polymers in solution, this work focuses on the properties of these macromolecules in the melt away from equilibrium. Hyperbranched polymers were simulated over a wide range of strain rates so the change in the behaviour of these polymers under shear, including different structural and rheological properties, can have been analysed. Figure 5.5 illustrates the changes in shape and orientation of hyperbranched polymers with 187 monomers at the strain rates of 0.0001, 0.001, 0.01 and 0.1. It can be seen that at higher strain rates, hyperbranched polymer molecules are more stretched, as is to be expected.

## 5.2. Radius of gyration

The mean square radius of gyration of molecules, which is a measure of the extension of a molecule in space, can be calculated according to the formula:

$$\langle \mathbf{R}_g \mathbf{R}_g \rangle \equiv \left\langle \frac{\sum_{\alpha=1}^{N_s} m_{\alpha} (\mathbf{r}_{\alpha} - \mathbf{r}_{CM}) (\mathbf{r}_{\alpha} - \mathbf{r}_{CM})}{\sum_{\alpha=1}^{N_s} m_{\alpha}} \right\rangle \quad (5.4)$$

where  $\mathbf{r}_{\alpha}$  is the position of bead  $\alpha$ ,  $\mathbf{r}_{CM}$  is the position of the molecular centre of mass and the angle brackets denote an ensemble average. The value of the squared radius of gyration is defined as the trace of the tensor ( $R_g^2 = Tr(\langle \mathbf{R}_g \mathbf{R}_g \rangle)$ ). These simulated values are often compared to experimental results using light scattering, small-angle neutron scattering and small-angle X-ray scattering methods which are well-established in polymer science. In this work, as only idealized hyperbranched architectures with one specific imperfect point are examined, the radius of gyration results cannot be compared directly to experimental data for a randomly branched polydisperse system. However the analysis of the radius of gyration gives significant information about the mean spatial distribution inside the molecules regardless of their shapes.

### 5.2.1. Radius of gyration of hyperbranched polymers with different molecular weights

Figure 5.6 presents the dependence of the radii of gyration for the type A hyperbranched polymers of different molecular weights on strain rate. For all studied systems, at small

strain rates, the size of the polymer remains constant but for large values of strain rate, the values of  $\langle R_g^2 \rangle$  increase which indicates that molecules are stretched under shear. For a given value of strain rate, the extent of shear induced stretching increases with the number of beads. In order to compare the results for the type A hyperbranched polymers to those for dendrimers (Bosko et al., 2004a) and linear polymers, the values of the mean square radii of gyration for these polymers are plotted against the strain rate as shown in Figure 5.7. As can be seen, the radii of gyration for hyperbranched polymers are always in the range between those of dendrimers and linear polymers. This can be explained by the architecture of the molecules. With the same number of monomers, dendrimer structures on average have the most compact geometry with the smallest spatial separation of monomers, whereas hyperbranched polymers are less compact while linear polymers have the largest distances between monomers.

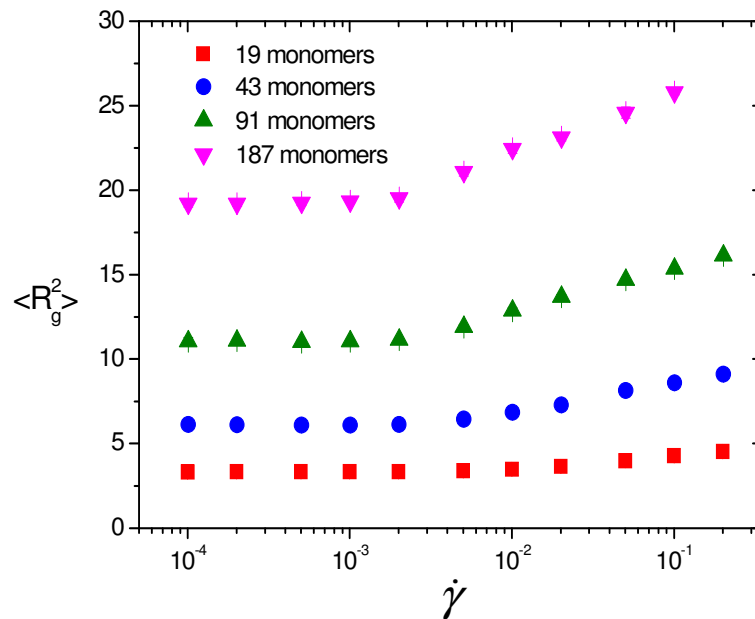


**Figure 5.6.** Mean squared radii of gyration of the type A hyperbranched polymers of different molecular weights at different strain rates.

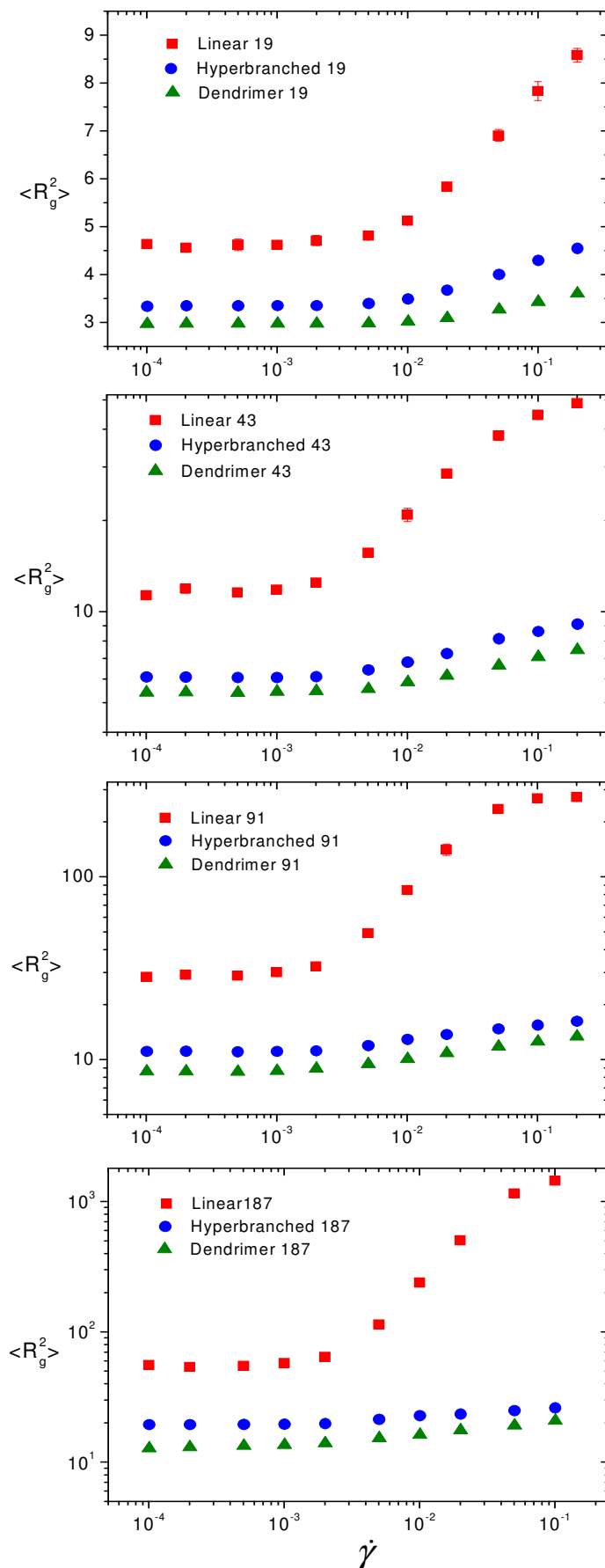
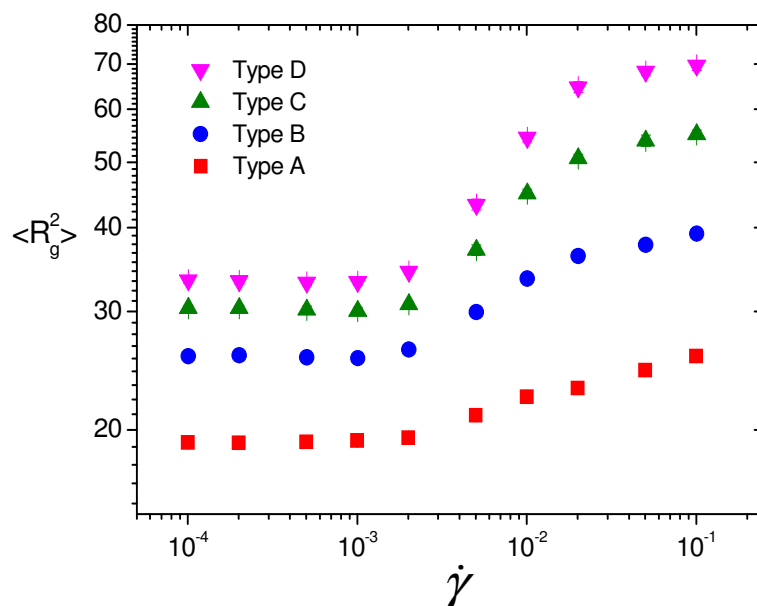


Figure 5.7. Comparison of radii of gyration for type A hyperbranched polymers, dendrimers and linear polymers.

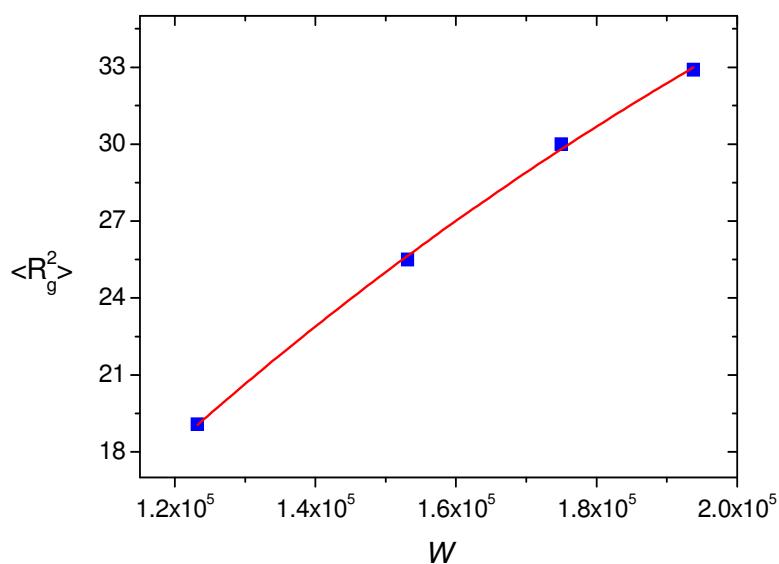
### 5.2.2. Radius of gyration of hyperbranched polymers with different numbers of spacers

Figure 5.8 presents the mean squared radius of the gyration for hyperbranched polymers with the number of beads per molecule of 187 but different numbers of spacers. At low strain rates, the value of  $\langle R_g^2 \rangle$  remains constant while at high strain rates where the molecules are stretched,  $\langle R_g^2 \rangle$  increases rapidly. Furthermore as type A molecules have the most dense and rigid structure while type D molecules have the most open and flexible architecture, the radius of gyration rises the least steadily for type A hyperbranched polymers and the most steadily for type D polymers. The ratio of the radii of gyration at strain rates of 0.0001 and 0.1 is 1.34 for type A, 1.52 for type B, 1.81 for type C and 2.08 for type D polymers. In addition, hyperbranched polymers of type A have the most compact architecture with the least extension of molecules in space. Hence at a given strain rate, the radius of gyration is lowest, whereas hyperbranched polymers of type D with the greatest spatial separation of beads have the highest value of the radius of gyration.



**Figure 5.8.** Dependence of the radius of gyration on strain rate for hyperbranched polymers with the same molecular weight of 187 beads but different numbers of spacers.

Data for the radii of gyration for different hyperbranched polymers were fitted using the Carreau-Yasuda model (Bird et al., 1987) which is usually used for viscosity data, given as  $\langle R_g^2 \rangle = \langle R_g^2 \rangle_0 / \left[ 1 + (\lambda_{R_g} \dot{\gamma})^2 \right]^{p_{R_g}}$  where  $\lambda_{R_g}$  is a time constant and  $p_{R_g}$  is the power law exponent. Results for the zero shear rate radii of gyration were plotted against the Wiener index as shown in Figure 5.9. The exponential function gives a very good fit to the zero shear rate mean square radius of gyration data. The dependence of  $\langle R_g^2 \rangle_0$  on the Wiener index was found to be  $\langle R_g^2 \rangle_0 = 61(15) - 85(5) \times e^{-W/18(8) \times 10^4}$  where the number in brackets shows the statistical uncertainty from the standard error of the fit.



**Figure 5.9. Dependence of zero shear rate radii of gyration on Wiener index for 187 bead hyperbranched polymers with different numbers of spacers (the solid line representing fitting with the exponential function).**

The relationship between the radius of gyration and molecular weight for dendrimers was suggested to be a complex function of the generation number, the order of the dendra and the functionality of the core (LaFerla, 1997). However for hyperbranched polymers, the power law scaling is the most common approach because of its sufficiency in characterizing the dependence of the radius of gyration on molecular weight for hyperbranched polymers with different levels of imperfectness or irregularity. If a power law function is used to fit the  $\log \langle R_g^2 \rangle_0$  data, the zero shear rate mean squared radius of gyration scales as  $\langle R_g^2 \rangle_0 \propto W^{1.20(6)}$ . The power law exponent of

1.20(6) for these hyperbranched polymers in NEMD simulations is close to the value of 1.0 found for phantom chains neglecting long-range excluded volume interactions and the correction term  $R(n_{ij})$  in the calculation of the end-to-end distance between two segments. This correction term is given as  $\langle R_g^2 \rangle_0 = C_\infty n_{ij} \langle I^2 \rangle + R(n_{ij})$  where  $C_\infty$  is the characteristic ratio of an infinite chain,  $n_{ij}$  is the number of bonds between segments  $i$  and  $j$  and  $\langle I^2 \rangle$  is the mean-squared bond length (Widmann and Davies, 1998). Brownian dynamics simulations (Neelov and Adolf, 2004, Sheridan et al., 2002) which take into account the excluded volume and hydrodynamic interactions also showed a power law exponent of approximately 1.0 for hyperbranched polymers of different molecular weights. Specifically the Brownian dynamics results showed that the zero shear rate radius of gyration scales as  $\langle R_g \rangle_0 \sim W^{0.5} N_s^{-0.85}$  which means that the squared radius of gyration scales as  $\langle R_g^2 \rangle_0 \sim W \times N_s^{-1.7}$ . It is interesting that this relationship for hyperbranched polymers is very similar to that for linear chains in good solvents  $\langle R_g^2 \rangle_0 \sim W \times N_s^{-1.824}$  which results from  $W \sim N_s^3$  for linear polymers and  $\langle R_g \rangle_0 \sim N_s^{0.588}$  for linear molecules in good solvents (Doi and Edwards, 1986). In ideal solvents or melts, the squared radius of gyration for linear polymers scales as  $\langle R_g^2 \rangle_0 \sim N_s$  hence the relationship between  $W$ ,  $R_g$  and  $N_s$  is expected to be  $\langle R_g^2 \rangle_0 \sim W \times N_s^{-2.0}$ . Furthermore, it was found that at high elongation rates, the dependence of the limiting (plateau) mean squared radius of gyration on Wiener index for hyperbranched polymers is close to  $W^3$  (Neelov and Adolf, 2004).

In order to clarify the relationship between  $W$ ,  $R_g$  and  $N_s$ , radius of gyration data for the type A hyperbranched polymers with different molecular weights in Figure 5.6 were fitted using the Carreau-Yasuda equation and the zero shear rate radii of gyration were plotted against the number of beads per molecule, as shown in Figure 5.10. The dependence of  $R_g$  on  $N_s$  was found to be  $\langle R_g^2 \rangle_0 \propto N_s^{0.773(6)}$ . On the other hand, the Wiener index for these systems scales as  $W \propto N_s^{1.6(1)}$ , as presented in Figure 5.11. Therefore the relationship between  $W$ ,  $R_g$  and  $N_s$  for the short branch polymer

molecules simulated is  $\langle R_g^2 \rangle_0 \sim W \times N_s^{-0.9}$ . Taken together these results shows that more work is needed to understand the relationship between the Wiener index, radius of gyration and molecular weight for hyperbranched polymers.

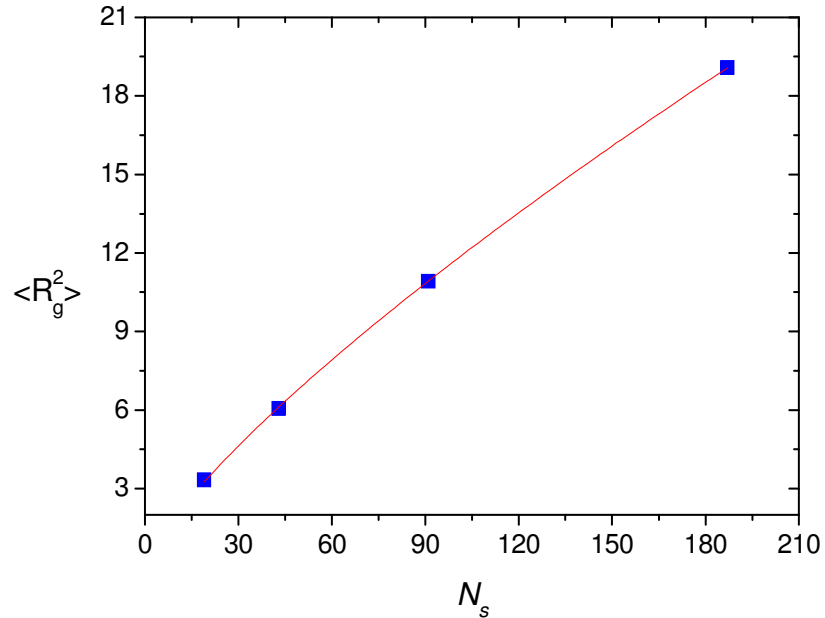


**Figure 5.10.** Dependence of zero shear rate radii of gyration on the number of beads per molecule for type A hyperbranched polymers.

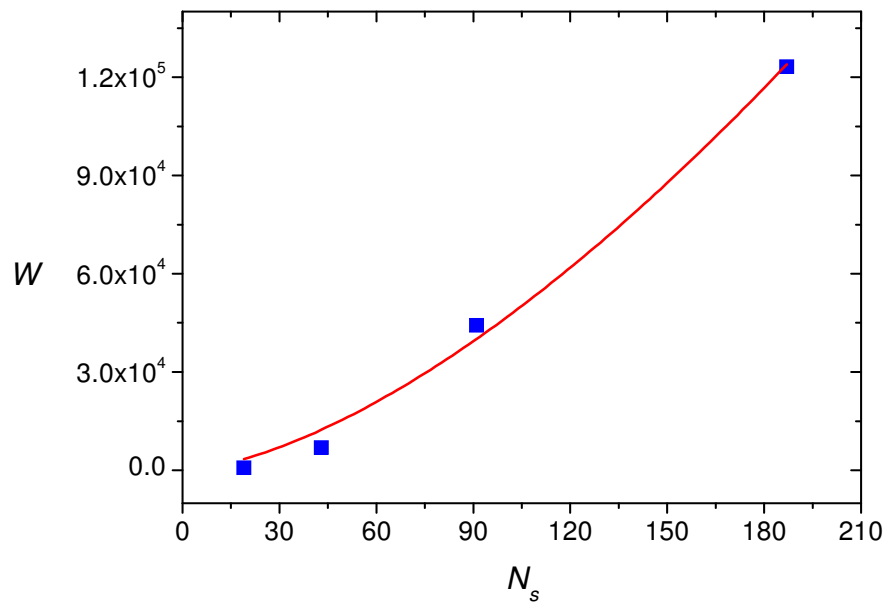


**Figure 5.11.** Dependence of the Wiener index on the number of beads per molecule for short branch hyperbranched polymers of type A.

### 5.2.3. Radius of gyration of blends composed of hyperbranched polymers and linear chains of equivalent molecular weight

As hyperbranched polymers have a promising application as rheology modifiers, blends of these polymers and linear chains have been simulated in this work. Hyperbranched polymers of type A and D comprising 187 beads per molecule were mixed with linear analogues of the same molecular weight. The proportions of hyperbranched polymers in these mixtures were chosen to be 4%, 8%, 12%, 16% and 20%. The simulation box contains 125 molecules in which 5, 10, 15, 20 and 25 molecules respectively are hyperbranched polymers of type A or D.

Figure 5.12 shows the mean squared radii of gyration for blends comprising 187 bead type A or D hyperbranched polymers and linear chains of equivalent molecular weight at different strain rates. For all blends, the radii of gyration remain constant at low strain rates and increase rapidly at high strain rates. Furthermore an increase in the proportion of hyperbranched polymers in the blends leads to a decrease in the value of the squared radius of gyration due to the compact structure of hyperbranched molecules. On the other hand, the presence of type A hyperbranched polymers in the blends reduces the mean squared radii of gyration of the system more than that of type D polymers. This is in accordance with the smaller values of  $\langle R_g^2 \rangle$  for type A hyperbranched polymers in comparison with that for type D polymers at all strain rates considered as discussed in the previous section. The radius of gyration data for blends of hyperbranched and linear polymers were fitted with the Carreau – Yasuda equation and results on the zero shear rate squared radius of gyration are presented in Table 5.2. Furthermore the mean squared radii of gyration for only linear chains or only hyperbranched polymers in the blends do not differ from those for pure linear chain melts or pure hyperbranched polymer melts.

**Table 5.2. Zero shear rate radii of gyration for blends of 187 bead hyperbranched and linear polymers**

Hyperbranched polymer fraction in blends	Type A	Type D
4%	49(7)	50(6)
8%	48(6)	49(7)
12%	47(6)	48(6)
16%	45(6)	47(6)
20%	44(5)	45(6)

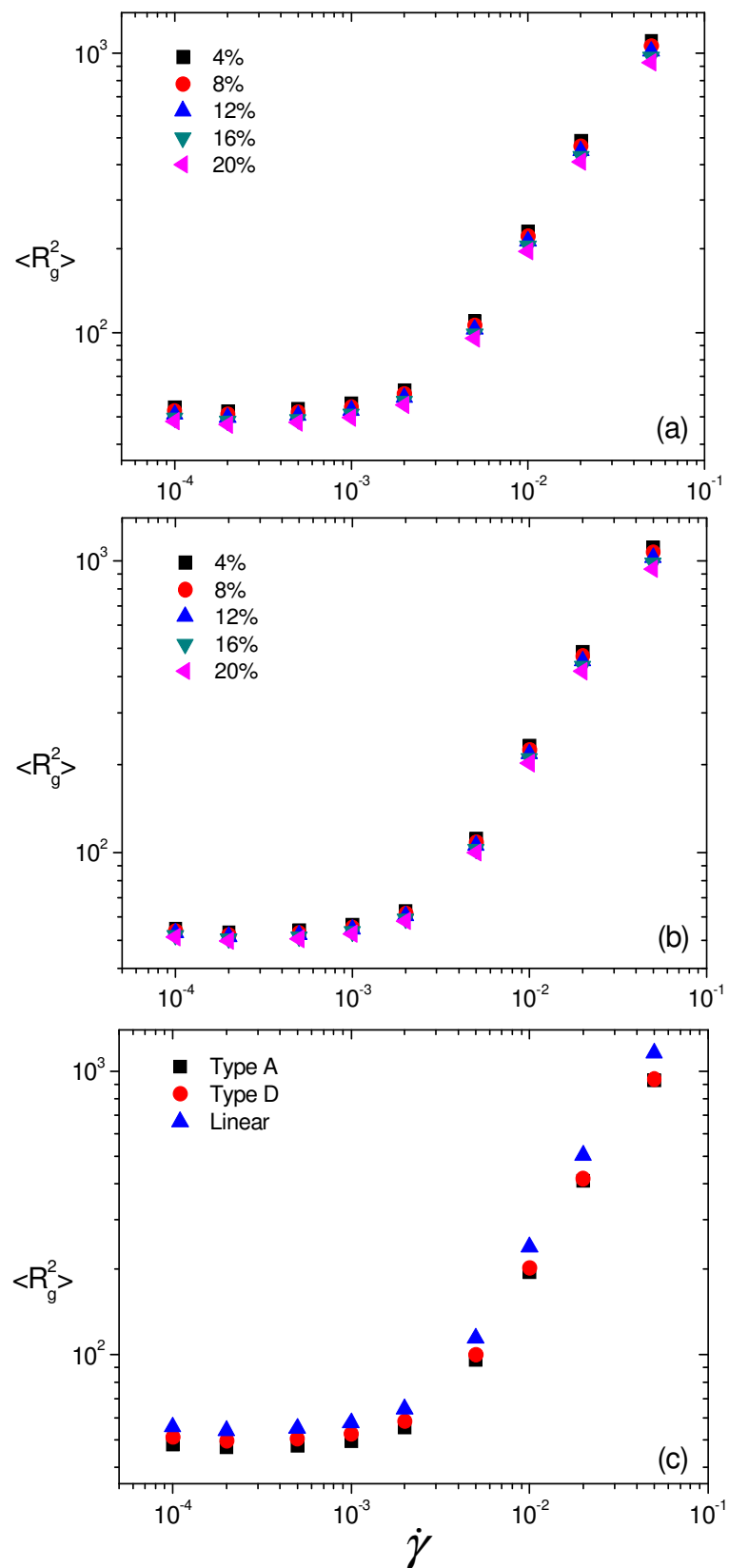


**Figure 5.12.** Mean squared radii of gyration for blends of 187 bead linear polymers and hyperbranched polymers of (a) type A, (b) type D with different hyperbranched polymer fractions and (c) type A and D with hyperbranched polymer fraction of 20% and squared radii of gyration for pure 187 bead linear polymers.

### 5.3. Tensor of gyration

The tensor of gyration is a useful parameter to characterize the structural properties and alignment of molecules. By studying the tensor of gyration, the shape of hyperbranched polymers can be investigated. The ensemble averaged eigenvectors and eigenvalues ( $L_1$ ,  $L_2$  and  $L_3$ ) of the tensor of gyration were derived to analyse flow-induced changes in the shape of the molecules, as the flow induced stretching of hyperbranched polymers together with molecular alignment can lead to the macroscopic anisotropy of the material (Bosko et al., 2004a). In order to calculate these ensemble averaged eigenvalues, the tensor of gyration was diagonalized separately for each molecule in the system. Using this approach, the shape of the hyperbranched polymer molecule can be studied disregarding the molecular orientation. The ratios of these eigenvalues, which describe the asymmetry of hyperbranched polymers, were also calculated. Results of the ensemble averaged tensor of gyration prior to its orthogonalization have also been computed and the corresponding eigenvalues ( $L'_1$ ,  $L'_2$  and  $L'_3$ ) were analyzed. In this approach, all elements of the tensor of gyration are averaged over all molecules and time separately, the shape of a mean molecule is obtained from superposition of all molecules in the system and these eigenvalues can be considered as the linear dimensions of the ellipsoid occupied by the orientationally averaged molecule (Bosko et al., 2006).

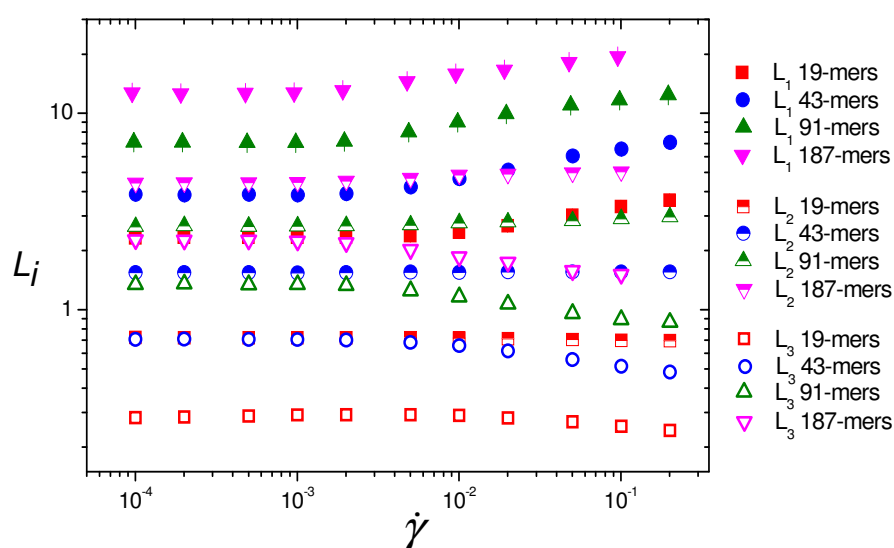


**Figure 5.13.** Averaged eigenvalues of the tensor of gyration for type A hyperbranched polymers of different molecular weights.

As mentioned above, the mean shape of a polymer molecule in the system is characterized by the ensemble average eigenvalues  $L_1$ ,  $L_2$  and  $L_3$  of the tensor of gyration which was diagonalized separately for each molecule. These values were computed for hyperbranched polymers of different molecular weight and plotted against the strain rate. As shown in Figure 5.13, for all type A hyperbranched systems simulated, the values of  $L_1$  are always much higher than  $L_2$  and  $L_3$  which are very similar. This indicates that hyperbranched polymers have a prolate ellipsoid shape. In comparison with dendrimers and linear polymers (Bosko, 2005, Bosko et al., 2004a), the eigenvalues of the tensor of gyration for hyperbranched polymers are in the range between those of linear polymers and dendrimers but slightly higher than the eigenvalues for dendrimers. This shows that the prolate ellipsoid shape of hyperbranched polymer molecules is very similar to dendrimers but somewhat flatter. The variation of these values is related to the stretching of the molecules and becomes significant at high strain rates. The comparison of average eigenvalues of the tensor of gyration for different hyperbranched polymers is also presented. These values for hyperbranched polymers with different chain lengths show very similar trends.

The asymmetry of hyperbranched polymers is characterized by the ratios of the eigenvalues of the average gyration tensor. If the ratios of the eigenvalues are closer to 1, the molecules have greater spherical symmetry. Like dendrimers and linear polymers, hyperbranched polymer molecules are stretched under shear. The differences between the eigenvalues of the tensor of gyration increase with the increase in strain rates and there is a noticeable change in the slopes of these ratios at similar strain rates as can be seen in Figure 5.14. Previous investigations have shown that for dendrimers, with increasing number of beads, the molecules become more spherical and for linear polymers, an opposite trend is observed (Bosko et al., 2006). It is interesting that smaller molecules of hyperbranched polymers become aspherical under shear more slowly than larger molecules of hyperbranched polymers. In other words, small hyperbranched chains tend to retain their cross-section when stretched, while larger chains extend by contracting in their smallest dimension (i.e. they become flatter).

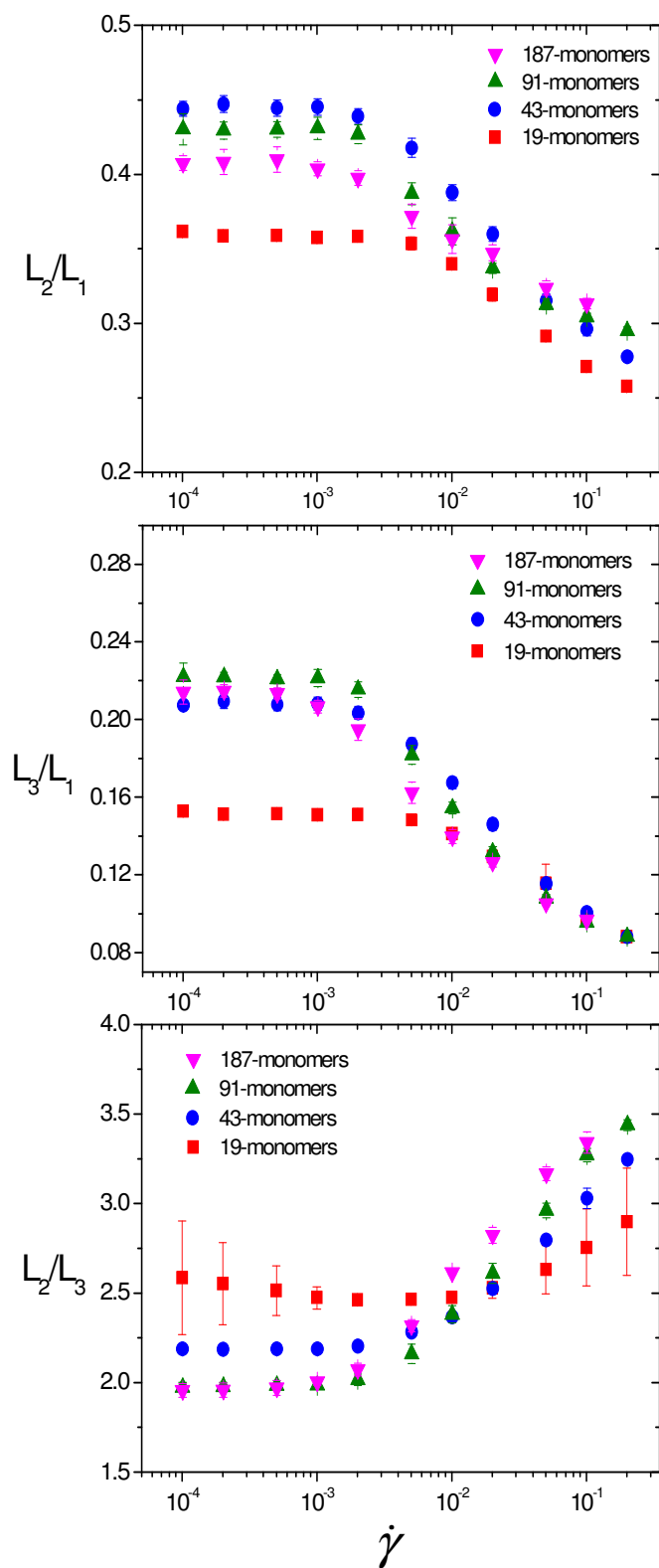
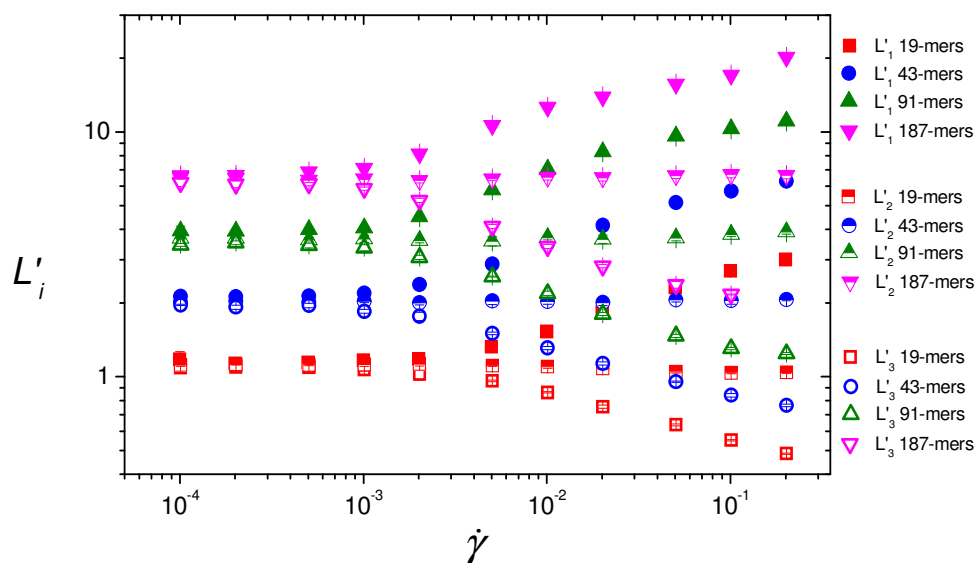


Figure 5.14. Ratios of averaged eigenvalues of the tensor of gyration for type A hyperbranched polymers with different molecular weights.



**Figure 5.15. Eigenvalues of the average tensor of gyration for type A hyperbranched polymers of different molecular weights.**

The eigenvalues of the average tensor of gyration for hyperbranched polymers, which was calculated prior to diagonalization, also reflect the degree of orientation of the molecules. They can be interpreted as the linear dimensions of the prolate ellipsoid occupied by the orientationally averaged molecule. For hyperbranched polymers, the eigenvalues of the average tensor of gyration are equal at equilibrium because of orientational disorder and depart from this equilibrium value right from the smallest strain rates, as shown in Figure 5.15. This demonstrates the onset of flow-induced molecular deformation. It can also be seen from Figure 5.14 that the eigenvalues of the average tensor of gyration for hyperbranched polymers of different size have very similar trends due to their similar behaviour under shear flow.

Ratios of the eigenvalues of the average tensor of gyration can be found in Figure 5.16. The ratios  $L'_2/L'_1$  and  $L'_3/L'_1$  both decrease with increasing strain rates. An opposite trend was observed for the ratio between  $L'_2$  and  $L'_3$  which increase with increasing strain rates. These behaviours are caused by the fact that hyperbranched polymers become more stretched along the flow axis and lead to the faster growth of  $L'_1$  with strain rates compared to the increase of  $L'_2$  and  $L'_3$ . These ratio values for hyperbranched polymers are again in the range between those for linear polymers and dendrimers due to their molecular topologies. Unlike the case of the average

eigenvalues of the tensor of gyration, the eigenvalues of the average tensor of gyration show very similar trends for dendrimers, linear and hyperbranched polymers.

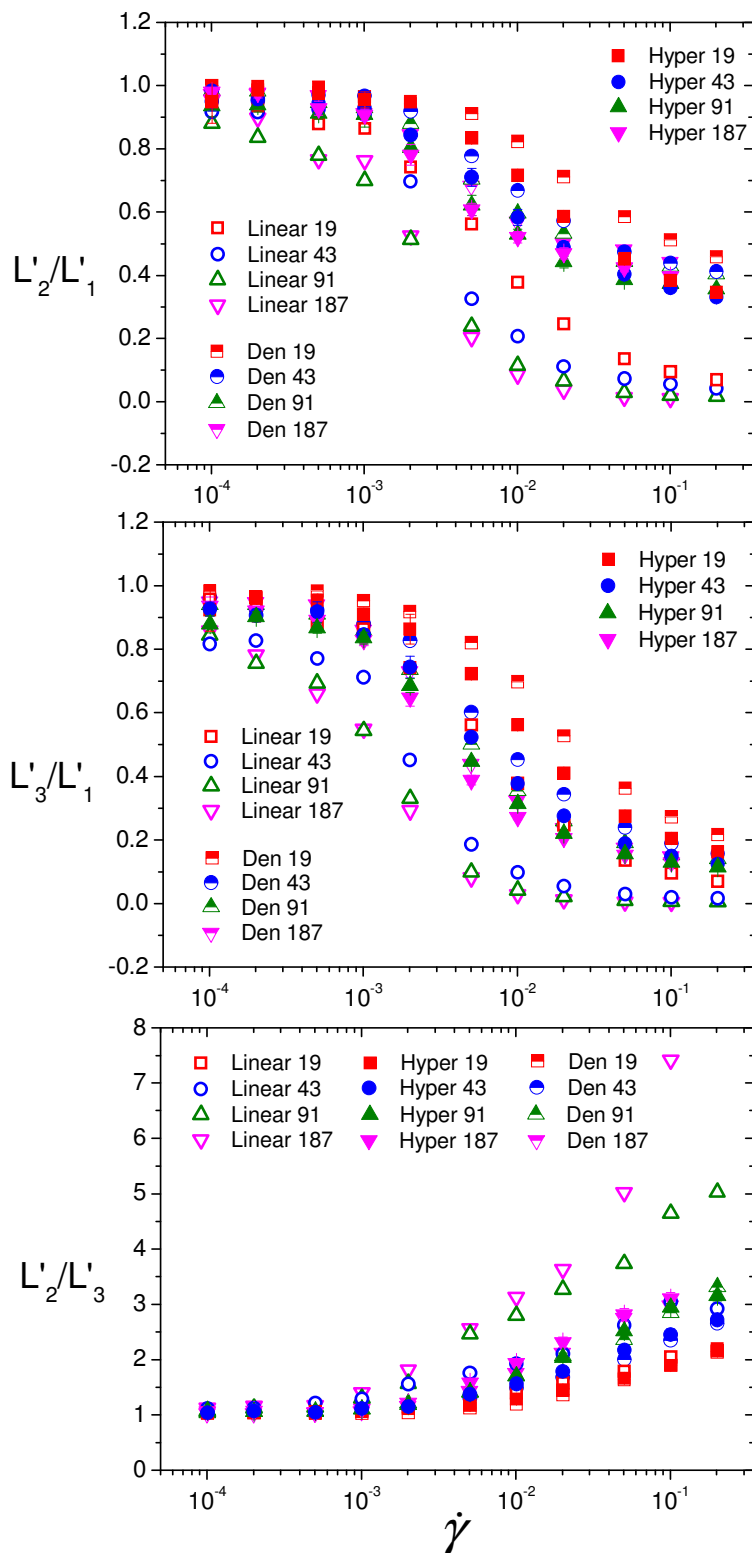


**Figure 5.16. Ratios of eigenvalues of the average tensor of gyration for type A hyperbranched polymers in comparison with those of dendrimers and linear polymers.**

### 5.4 Distribution of mass

Hyperbranched polymers have a compact, globular structure due to their densely branched architecture. This might lead to an unusual distribution of mass. To analyse the distribution of mass within the molecule, two forms of intra-molecular radial distribution function have been used. The first function, which measures the distribution of beads from the central bead (the core), is defined as:

$$g_{core}(r) = \frac{\left\langle \sum_{i=1}^N \sum_{\alpha=2}^{N_i} \delta(|\mathbf{r} - (\mathbf{r}_{i\alpha} - \mathbf{r}_{i1})|) \right\rangle}{N} \quad (5.5)$$

where  $\mathbf{r}_{i1}$  is the position of the core and  $\alpha$  runs over all other beads belonging to the same molecule. The second function, which measures the distribution of beads from the molecular centre of mass, is defined as:

$$g_{CM}(r) = \frac{\left\langle \sum_{i=1}^N \sum_{\alpha=1}^{N_i} \delta(|\mathbf{r} - (\mathbf{r}_{i\alpha} - \mathbf{r}_{CM})|) \right\rangle}{N} \quad (5.6)$$

where  $\mathbf{r}_{CM}$  is the position of the centre of mass.

#### 5.4.1. Distribution of mass for hyperbranched polymers of different molecular weights

The distribution of mass from the central unit (core) for different type A hyperbranched polymer systems at the strain rate of 0.0001 and 0.1 can be found in Figure 5.17, whereas the distribution of mass from the centre of mass at those strain rates is shown in Figure 5.18. In all cases, the distributions of mass for polymers with different chain lengths always show a similar trend. The correlation between the position of the core and its first neighbours expresses itself through a strong peak at the distance equal to the average bond length. At high strain rates, as the molecules are stretched in the flow, the distribution of mass becomes broader and the average distance of beads from the centre of mass increases with the strain rate. For the largest strain rates considered, the maximum distance between beads and the centre of mass is comparable to the lengths of fully stretched arms of the polymers.

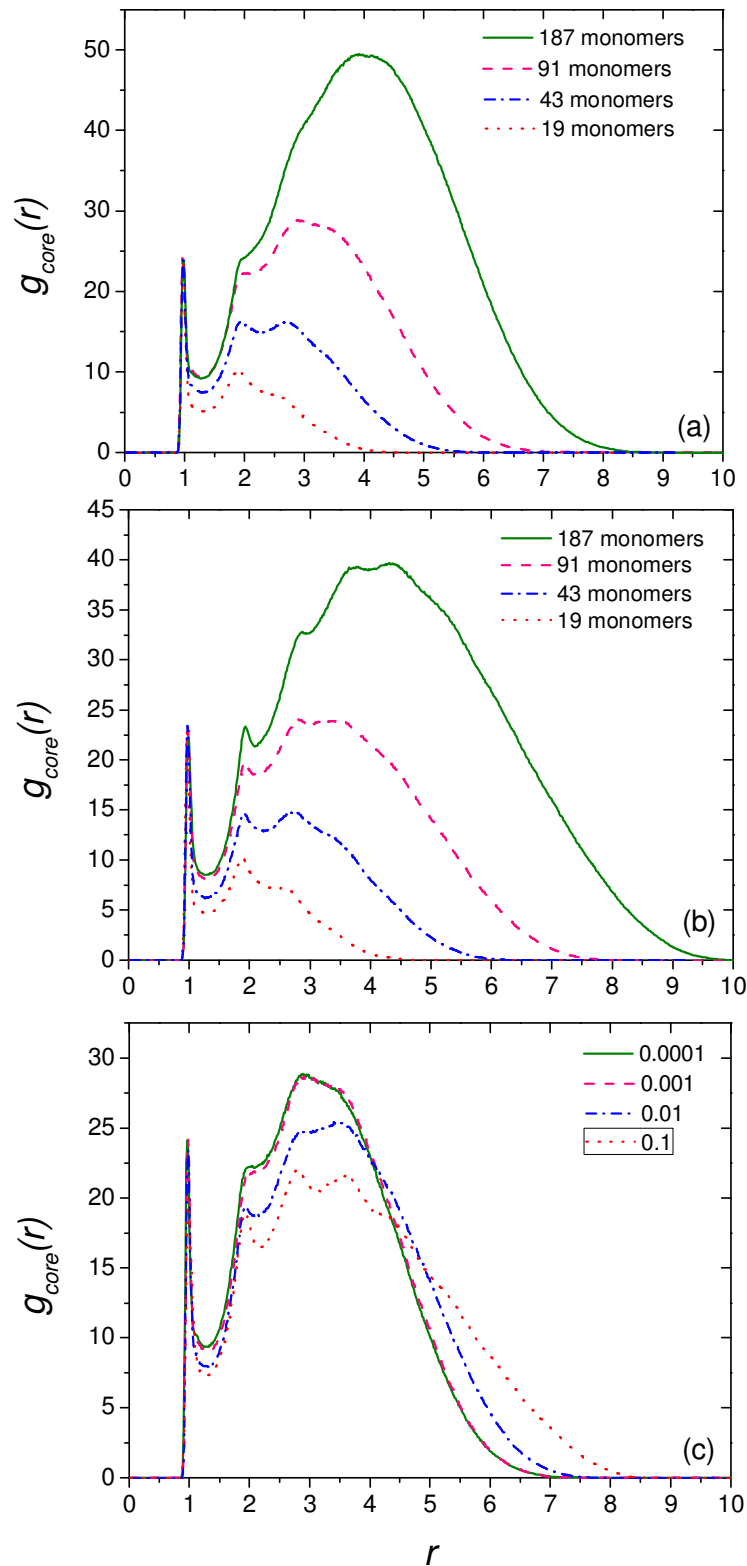


**Figure 5.17.** Distribution of beads from the core for type A hyperbranched polymers of different molecular weights at strain rates of (a) 0.0001, (b) 0.1 and (c) for type A hyperbranched polymers with 91 monomers at various strain rates.

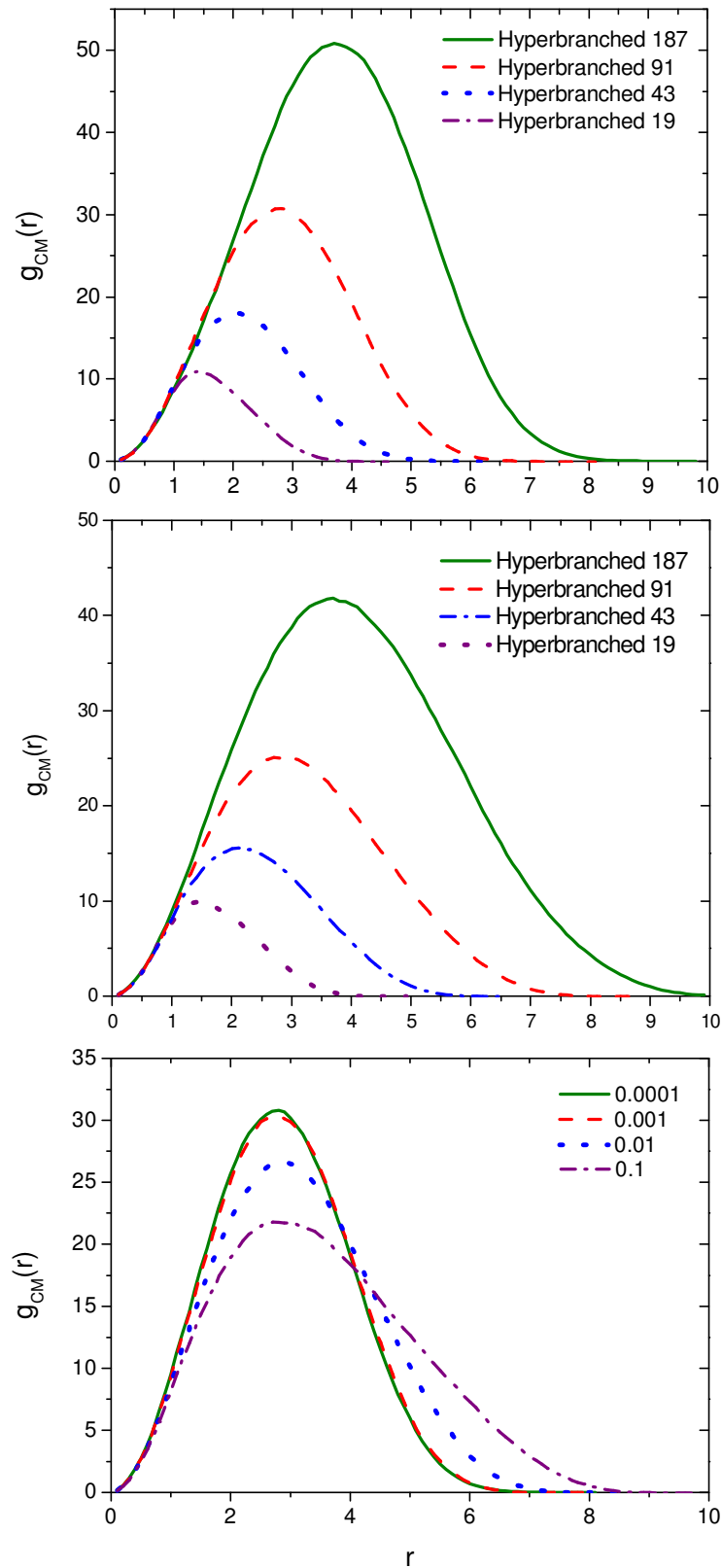
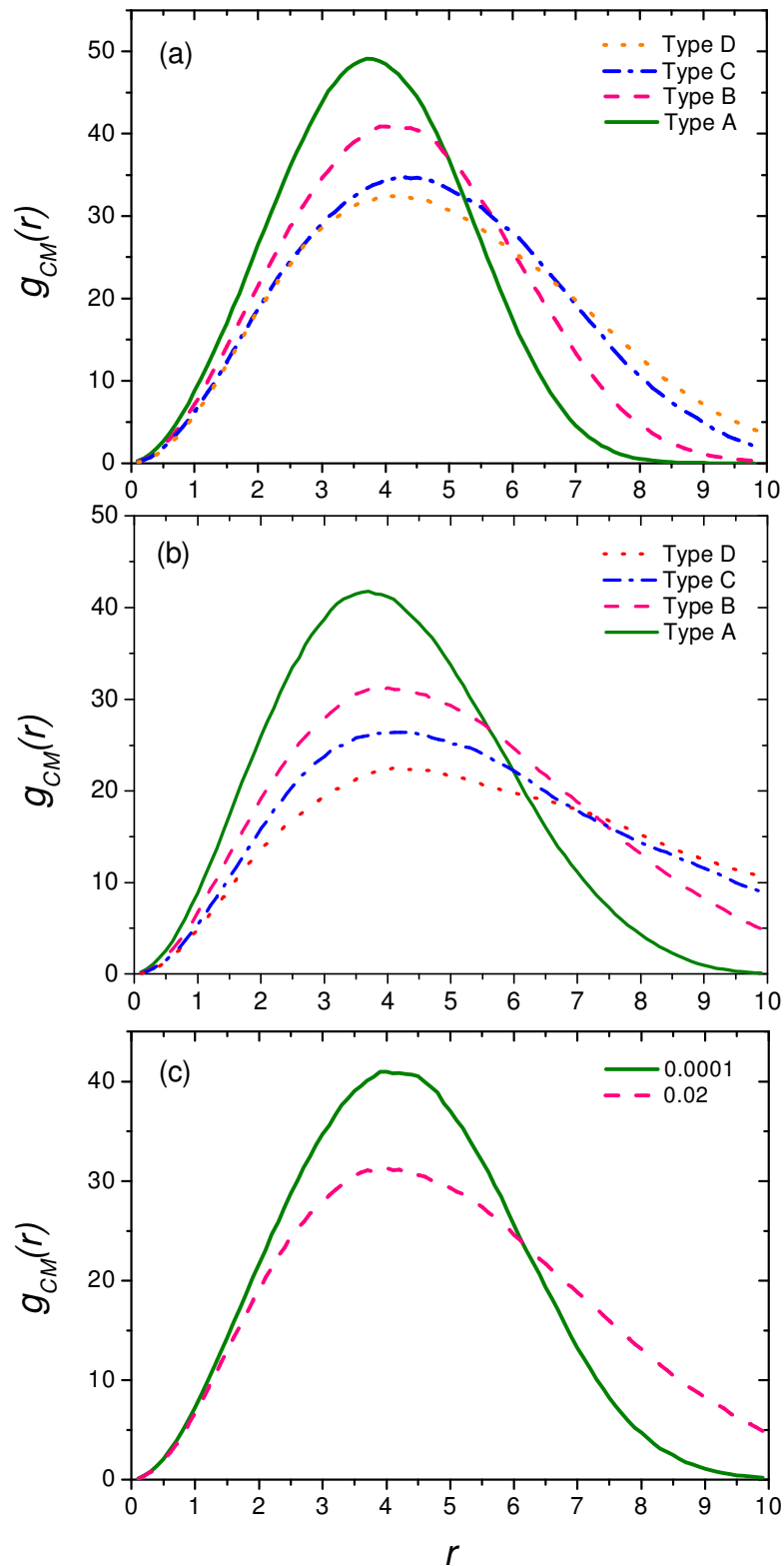


**Figure 5.18.** Distribution of beads from the centre of mass for type A hyperbranched polymers of different molecular weights at strain rates of (a) 0.0001, (b) 0.1 and (c) for type A hyperbranched polymers with 91 monomers at various strain rates.

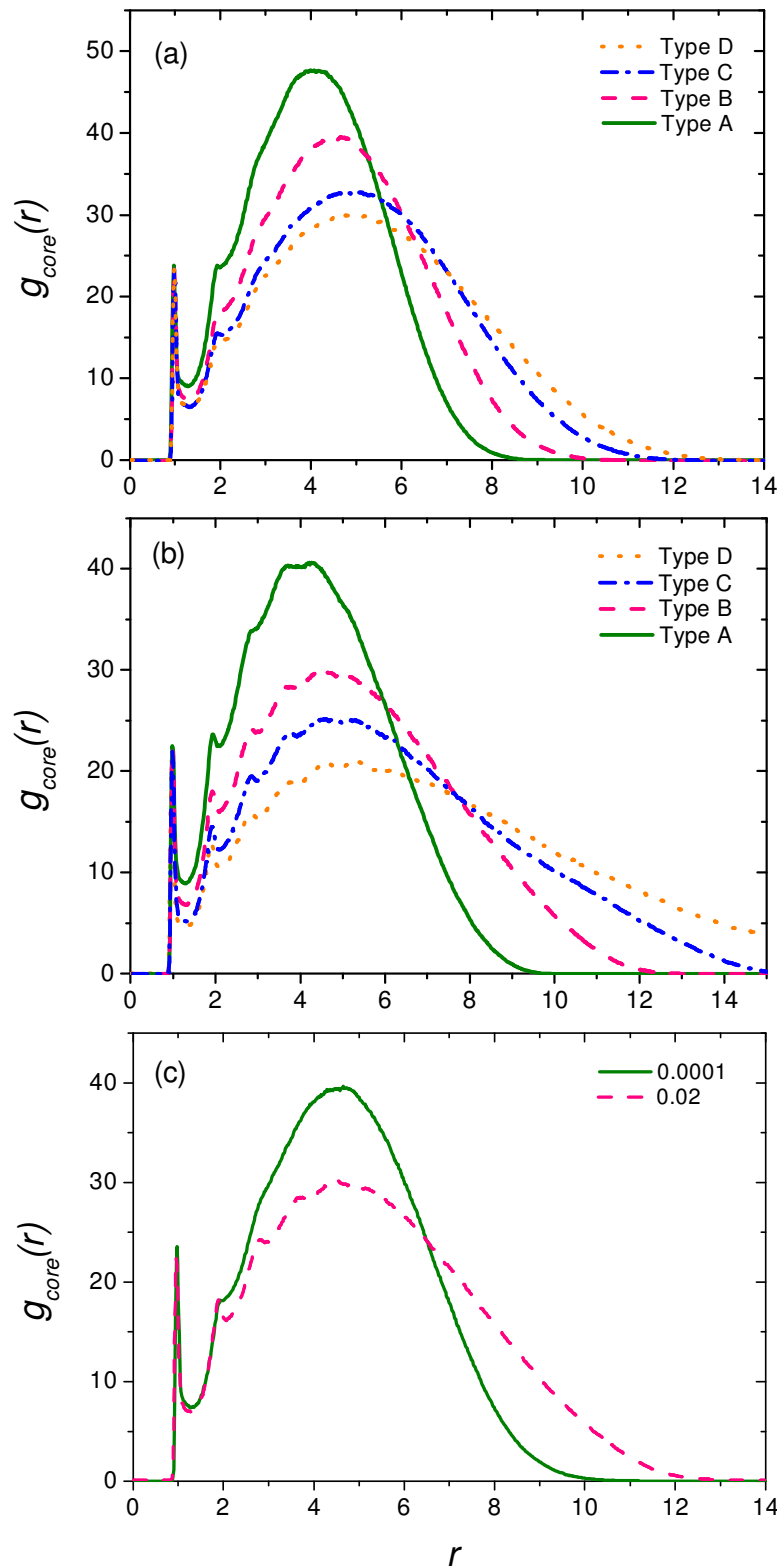
### *5.4.2. Distribution of mass for hyperbranched polymers with the same molecular weight of 187 beads but different numbers of spacers*

Figure 5.19 presents the distribution of beads from the molecular centre of mass for hyperbranched polymers of the same molecular weight of 187 beads but with different numbers of spacers. With increasing number of spacers, the distribution of mass becomes broader and the average distance of beads from the centre of mass increases. This is in accordance with the topologies of hyperbranched polymer systems simulated. Furthermore the shear-induced behaviour of the distribution of mass for different hyperbranched polymers shows a similar trend. At higher strain rates, the curves become wider and the peaks shift towards larger distance as molecules are stretched under shear flow. This behaviour was also observed in Brownian dynamics simulations for charged hyperbranched polymers (Dalakoglou et al., 2008).

The distribution of beads from the central bead (the core) for hyperbranched polymers with different numbers of spacers is presented in Figure 5.20. Strong peaks at the distance equal to the average bond length which are observed for all systems correspond to the first neighbours of the core. The same height of these peaks for different hyperbranched polymers is due to the same number of beads around the core in the inner-most shell of the molecules. In contrast, in the outer shells of the molecules, the separation of beads around the core is lowest for the system of type A and highest for the system of type D. Therefore the distribution of beads from the core is the most narrow for type A polymers and broadest for type D polymers. Similar to the radial distribution of beads from the centre of mass, the distribution of beads from the core for all hyperbranched polymers under shear flow becomes wider as molecules in the systems are stretched.



**Figure 5.19.** Distribution of mass from the centre of mass for hyperbranched polymers of the same molecular weight of 187 beads but with different numbers of spacers (a) at strain rate of 0.0001, (b) at strain rate of 0.02 and (c) hyperbranched polymer of type B at strain rate of 0.0001 and 0.02.



**Figure 5.20.** Distribution of mass from the core for hyperbranched polymers of the same molecular weight of 187 beads but with different numbers of spacers (a) at strain rate of 0.0001, (b) at strain rate of 0.02 and (c) hyperbranched polymer of type B at strain rate of 0.0001 and 0.02.

**5.4.3. Distribution of mass for blends of hyperbranched polymers and linear polymers of the equivalent molecular weight**

The distribution of beads from the centre of mass was computed for different blends of type A and type D hyperbranched polymers and linear chains of the same molecular weight of 187 beads. The distribution of beads from the centre of mass for blends comprising type A hyperbranched polymers is presented in Figure 5.21(a) whereas that for blends composed of type D hyperbranched polymers is shown in Figure 5.21(b). A comparison between the bead distribution functions of blends containing type A and type D hyperbranched polymers with the proportion of hyperbranched polymers of 20% can be found in Figure 5.21(c). All these results are for systems at the strain rate of 0.0001.

As can be seen from Figure 5.21(a), the distribution of beads from the centre of mass for blends composed of at least 12% type A hyperbranched polymers shows a peak at the distance of approximately 4 which is also the distance at which a peak is observed for the bead distribution function of pure type A hyperbranched polymers. The distribution of beads from the centre of mass for blends comprising less than 12% of the short branch type A hyperbranched polymers reaches the highest value when the distance  $r$  is about 5. At this distance from the centre of mass, the largest number of beads can be found in the melts of pure or blends mainly containing linear polymers.

In Figure 5.21(b), the distribution of beads from the centre of mass for blends composed of type D hyperbranched polymers is presented. A peak at the distance of approximately 5 is observed for blends with different ratios of hyperbranched and linear polymers. This is also the distance at which the largest number of beads is found for pure long branch type D hyperbranched polymers.

Figure 5.21(c) shows a clearer picture of the bead distribution functions for blends with the same proportion of hyperbranched polymers of type A or type D. As type A hyperbranched molecules have shorter branches and a larger number of branching points, a peak at a smaller distance from the centre of mass can be found.

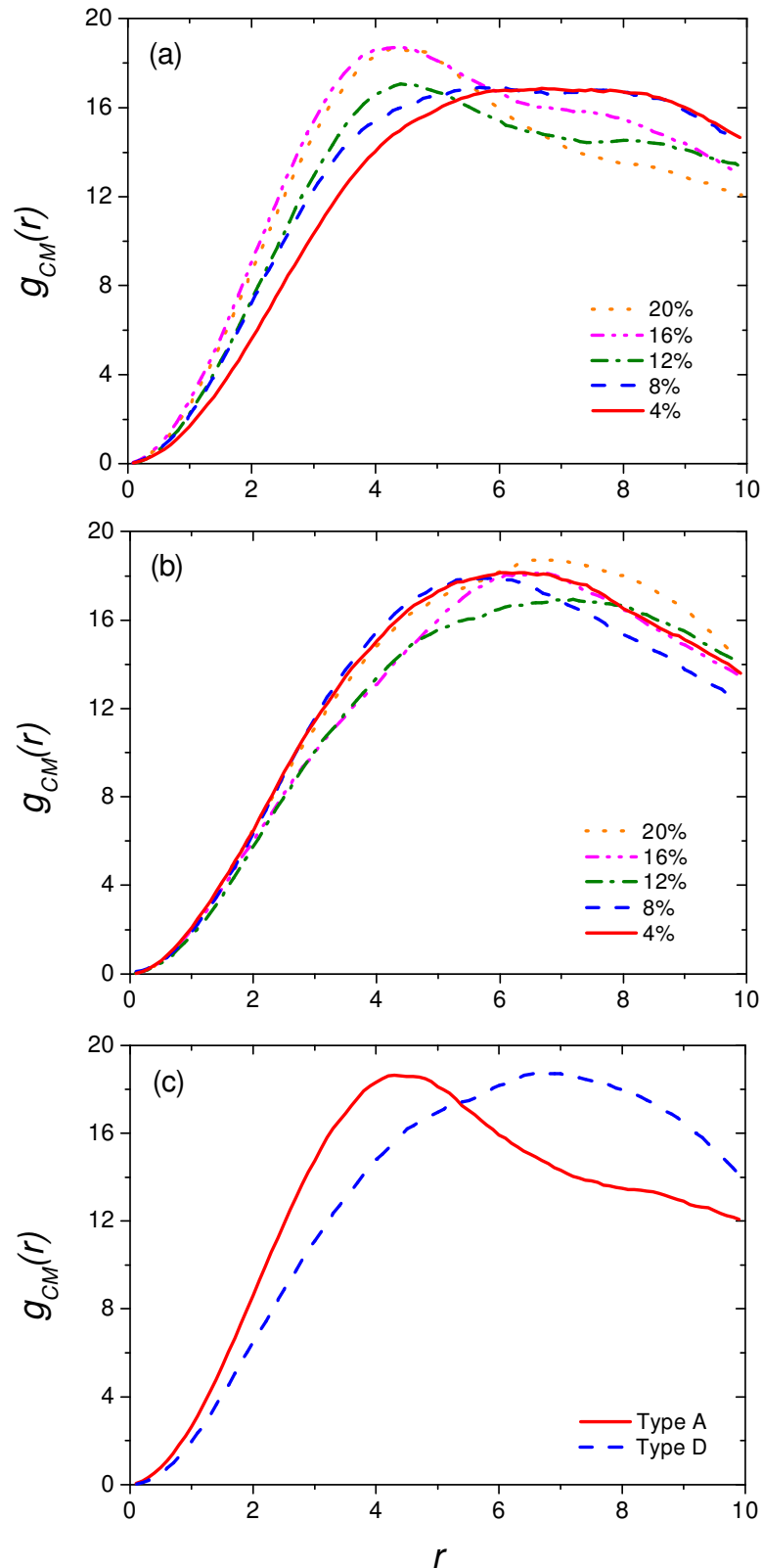


**Figure 5.21.** Distribution of mass from the centre of mass for blends of 187 bead hyperbranched polymers and linear chains of equivalent weight at strain rate of 0.0001. (a) Blends with different fractions of type A hyperbranched polymers, (b) Blends with different fractions type D hyperbranched polymers and (c) Blends with 20% hyperbranched polymers of type A or D.

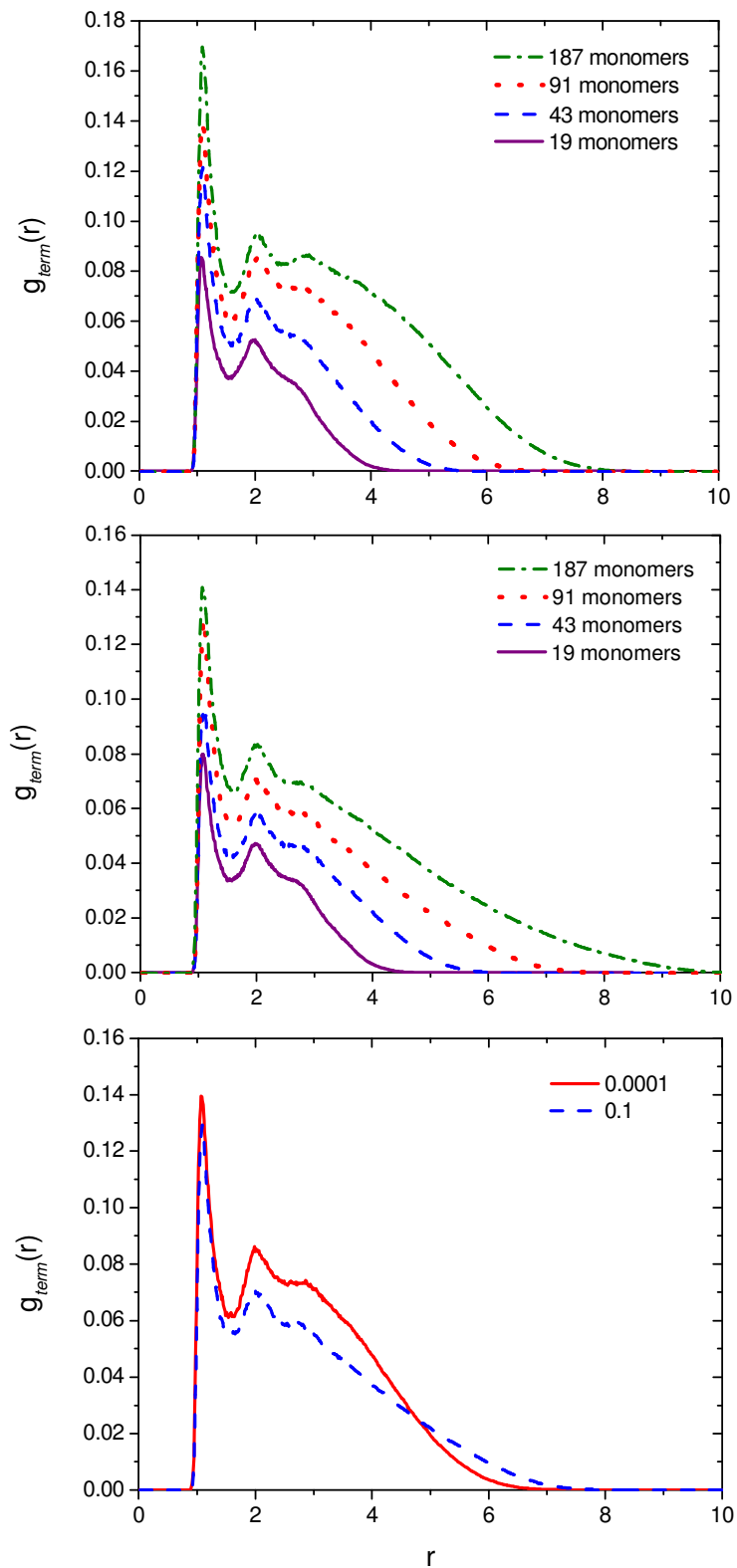


**Figure 5.22.** Distribution of terminal groups for type A hyperbranched polymers of different molecular weights at strain rates of (a) 0.0001, (b) 0.1 and (c) hyperbranched polymers with 91 beads at various strain rates.

### 5.5. Distribution of terminal groups

One of the special properties of hyperbranched polymers is the large number of terminal groups, from which hyperbranched polymers are characterized as active molecules. This leads to a number of applications, especially in drug delivery. Therefore, the radial distribution function of the terminal groups with reference to the central bead was also investigated to analyze the entanglement and back folding in the molecules. This is defined as:

$$g_{term}(r) = \frac{\left\langle \sum_{i=1}^N \sum_{\alpha \in \{term\}} \delta(|\mathbf{r} - (\mathbf{r}_{i\alpha} - \mathbf{r}_{i1})|) \right\rangle}{4\pi r^2 N} \quad (5.7)$$

where  $\alpha$  runs over the outermost beads only.

In Figure 5.22, we present the distribution of terminal groups from the central unit at the strain rate of 0.0001 when the system is close to equilibrium and at a high strain rate of 0.1 for type A hyperbranched polymers with different molecular weights. In all cases, the end groups can be found at any distance from the centre unit. This means that reactive groups exist everywhere throughout the interior of the molecules. Similar behaviour has been observed previously for dendrimers (Timoshenko et al., 2002, Lescanec and Muthukumar, 1990, Bosko et al., 2004a).

### 5.6. Atomic radial distribution function

The atomic radial distribution function is defined by:

$$g_A(r) = \frac{\left\langle \frac{1}{2} \sum_{i=1}^{N_{total}} \sum_{j \neq i}^{N_{total}} \delta(|\mathbf{r} - \mathbf{r}_{ij}|) \right\rangle}{4\pi r^2 N_{total} \rho} \quad (5.8)$$

where  $\mathbf{r}_{ij}$  is the distance between the beads  $i$  and  $j$ ,  $N_{total} = NN_s$  is the total number of beads in the studied system, and  $\rho$  is the density. It is extensively used to study the internal structure and spatial ordering of atoms (beads) composing materials. The function  $g_A(r)$  shows the probability of finding two beads at the separation  $r$ . The atomic

radial distribution simulation results can be directly compared to results of diffraction experiments.

The atomic radial distribution functions for hyperbranched polymers of different molecular weights as well as those for polymers of different numbers of spacers are indistinguishable. Therefore Figure 5.23 only shows the distribution function for polymers with different spacer lengths.

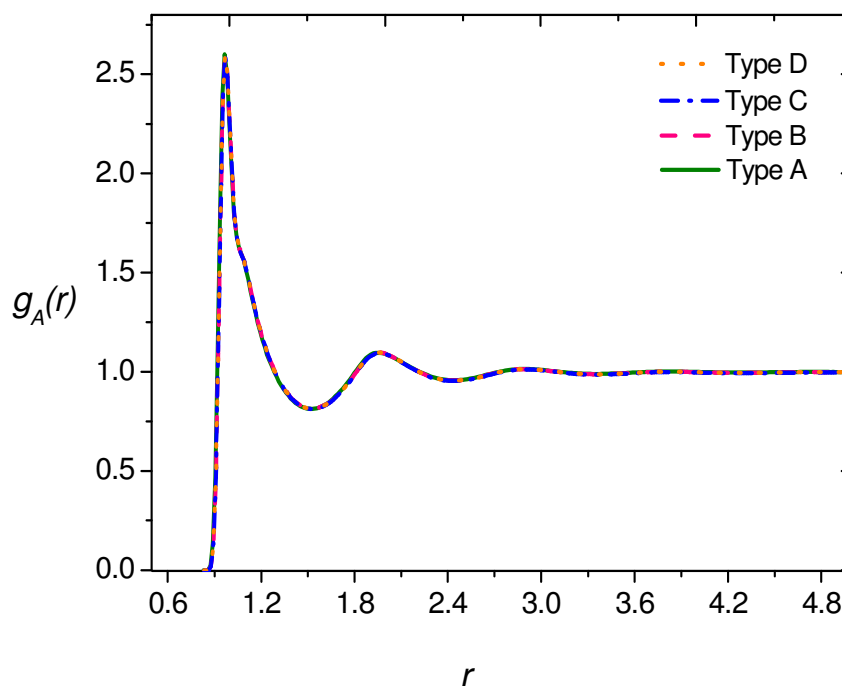


**Figure 5.23.** The atomic radial distribution function for 187 bead hyperbranched polymers with different numbers of spacers at the strain rate of 0.0001.

For blends of 187 bead hyperbranched polymers and linear chains of equivalent molecular weight, the atomic radial distribution functions are also not distinguishable when the proportion of hyperbranched molecules in the system changes. This can be seen from Figure 5.24.

The distribution function at different shear rates is shown in Figure 5.25. In all cases, only the first few peaks which correspond to the shells of near neighbours can be observed. No significant changes could be distinguished in the atomic radial distribution functions of hyperbranched polymers with their size, and the distributions of different hyperbranched polymers almost overlap. It can also be seen that the shear does not

significantly change the distribution function: the first peak becomes slightly wider whereas the second peak is shifted towards smaller distances. The first peak, which is also the strongest peak of the atomic radial distribution, consists of contributions from two types of first neighbours. The first type includes beads that are chemically bonded to the central one and interact via both WCA and FENE potentials, whereas the second type refers to all other beads that are close to the core and interact via only the WCA potential.

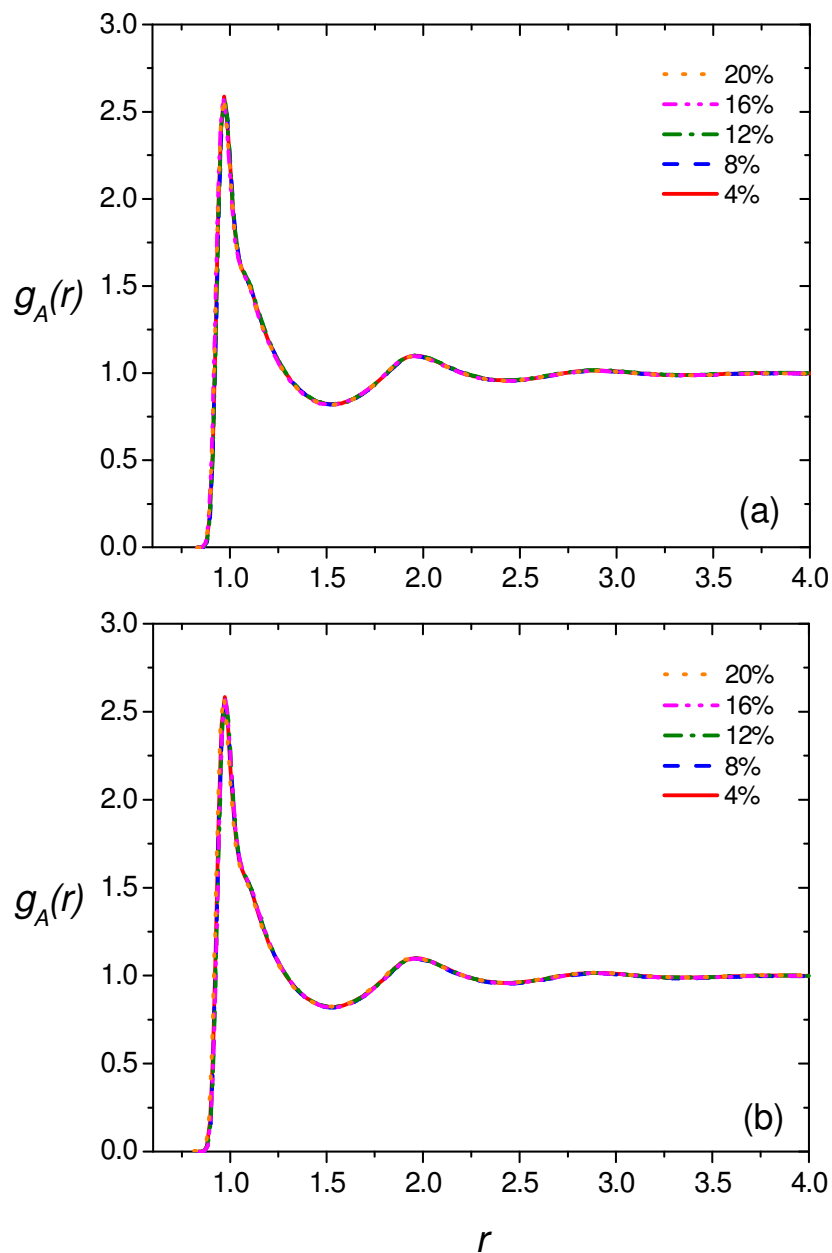


**Figure 5.24. Atomic radial distribution function for blends of 187 bead linear polymers and hyperbranched polymers of (a) type A and (b) type D.**

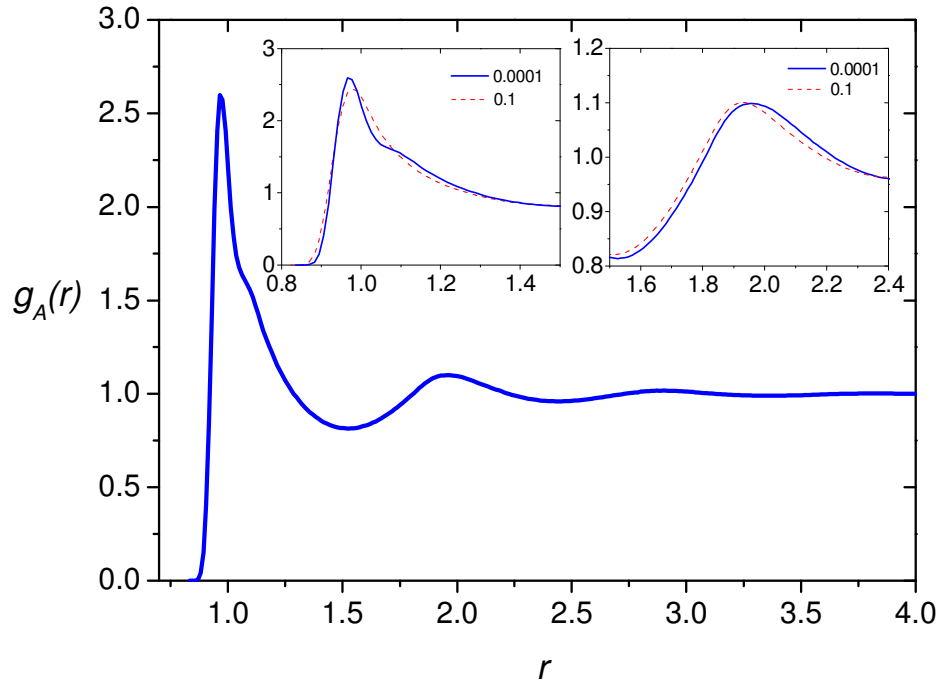


**Figure 5.25.** Atomic radial distribution function for type A hyperbranched polymer with 91 beads at strain rates of 0.0001 and 0.1.

## 5.7. Interpenetration

In order to characterize the interpenetration of the volume occupied by the molecule by beads of other molecules, the interpenetration function, defined as:

$$g_{inter}(r) = \frac{\left\langle \sum_{i=1}^N \sum_{j \neq i}^N \sum_{\alpha=1}^{N_j} \delta(|\mathbf{r} - (\mathbf{r}_{j\alpha} - \mathbf{r}_{i1})|) \right\rangle}{4\pi r^2 N} \quad (5.9)$$

where  $\mathbf{r}_{i1}$  is the position of the core of molecule  $i$  and  $\mathbf{r}_{j\alpha}$  is the position of bead  $\alpha$  in molecule  $j$ , was used and results are shown in Figures 5.26 and 5.27.

### 5.7.1. Interpenetration function for hyperbranched polymers of different molecular weights

As can be seen from Figure 5.26, the interpenetration function for hyperbranched polymers strongly depends on the molecular weight. The function decreases with

increasing number of beads per molecule. This is due to the architecture of these short branch polymers. With increasing molecular weight, the polymeric structure becomes more compact and the number of beads in the outer-most layers increases rapidly. Hence the bead density of these layers rises steadily and the interior becomes less accessible.

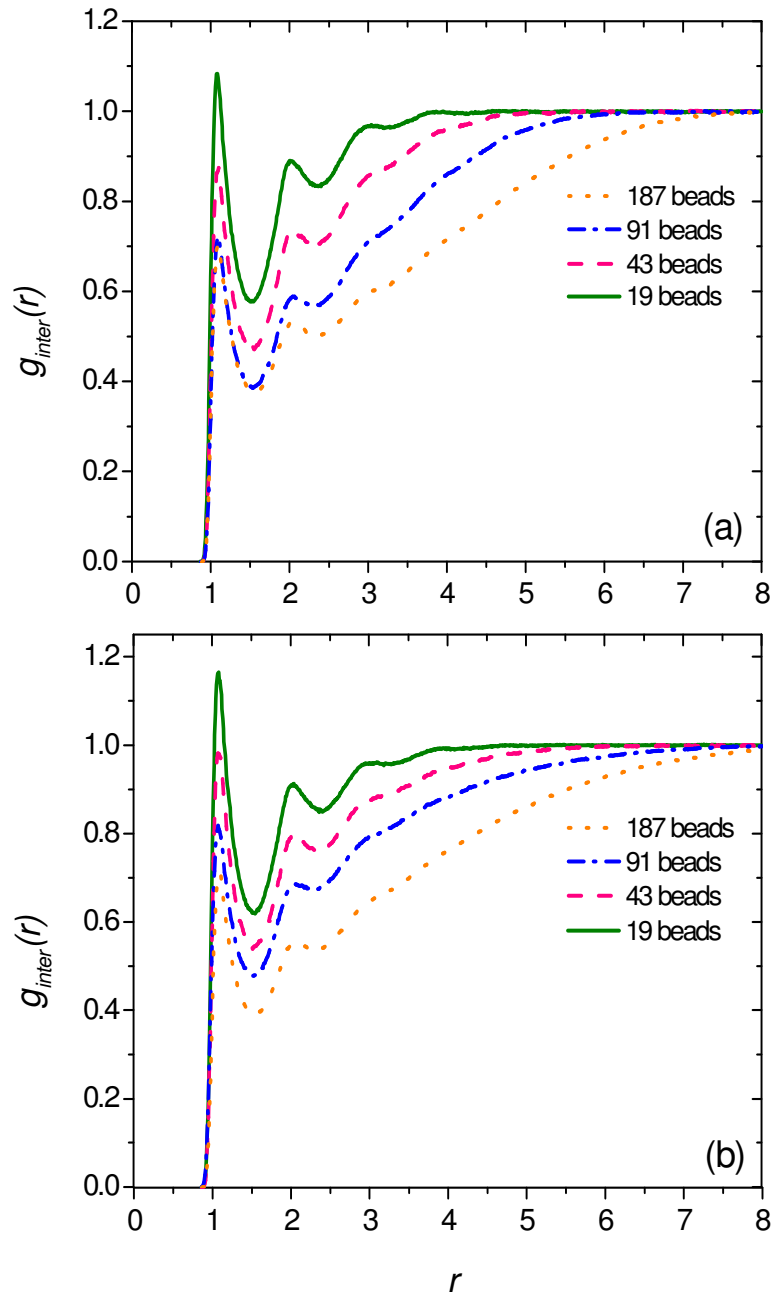


**Figure 5.26.** Interpenetration in the melts of type A hyperbranched polymers of different molecular weights at the strain rate of (a) 0.0001 and (b) 0.1.

### 5.7.2. Interpenetration function for hyperbranched polymers with different numbers of spacers

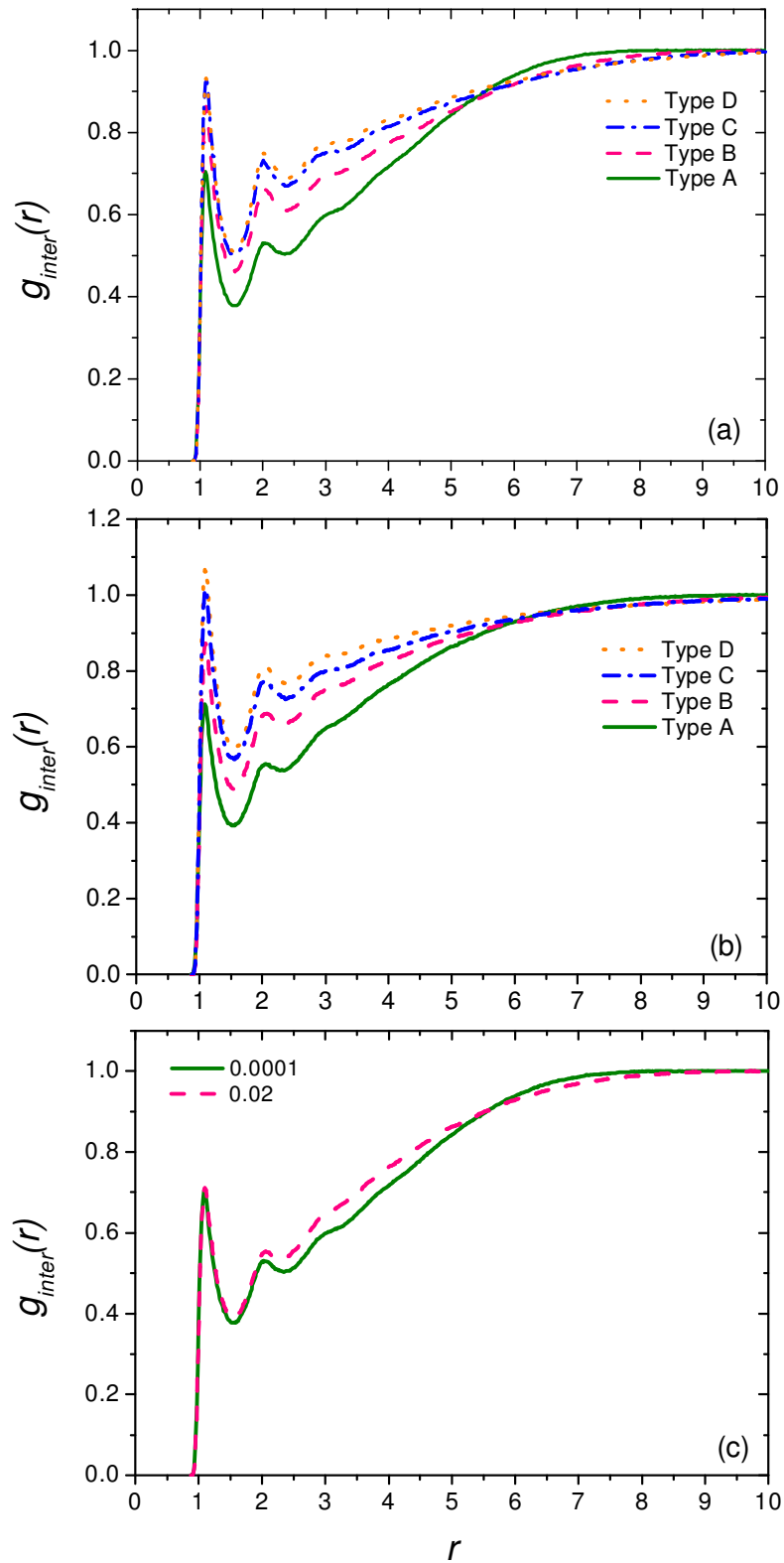


Figure 5.27. Comparison of the interpenetration function for hyperbranched polymers of the same molecular weight of 187 beads but with different numbers of spacers (a) at strain rate of 0.0001, (b) at strain rate of 0.02 and (c) type A hyperbranched polymer at strain rate of 0.0001 and 0.02.

In Figure 5.27, it can be clearly seen that the interpenetration function for hyperbranched polymers increases with the increase of the number of spacers. The system of type A has the lowest interpenetration function while the system of type D has the highest interpenetration function. This is because polymer molecules with longer linear chains between branching points are more open and freely accessible by beads of other molecules, whereas polymers with short chains between branching points have more compact structures which reduce the probability of finding parts of other molecules within the interior of a polymer molecule. Furthermore, under shear flow, the interpenetration increases with the increase of strain rate as molecules are stretched and become more open. Hence parts of other molecules can access closer to the core of the hyperbranched polymer molecule.

### **5.8. Flow birefringence**

In the presence of a velocity gradient, the statistical distribution of a flexible polymer is deformed from the equilibrium isotropic state and the refractive index of the medium becomes anisotropic. This phenomenon is called flow birefringence or the Maxwell effect. As mentioned in Chapter 3, the birefringence of a polymer system due to the alignment of the intramolecular bonds is called intrinsic birefringence whereas that caused by the alignment of the whole molecules is called form birefringence (Doi and Edwards, 1986). The contribution to the birefringence effect from the alignment of molecules is more important in the case of solutions and arises due to the differences between the polarisability of the molecules and the solvent.

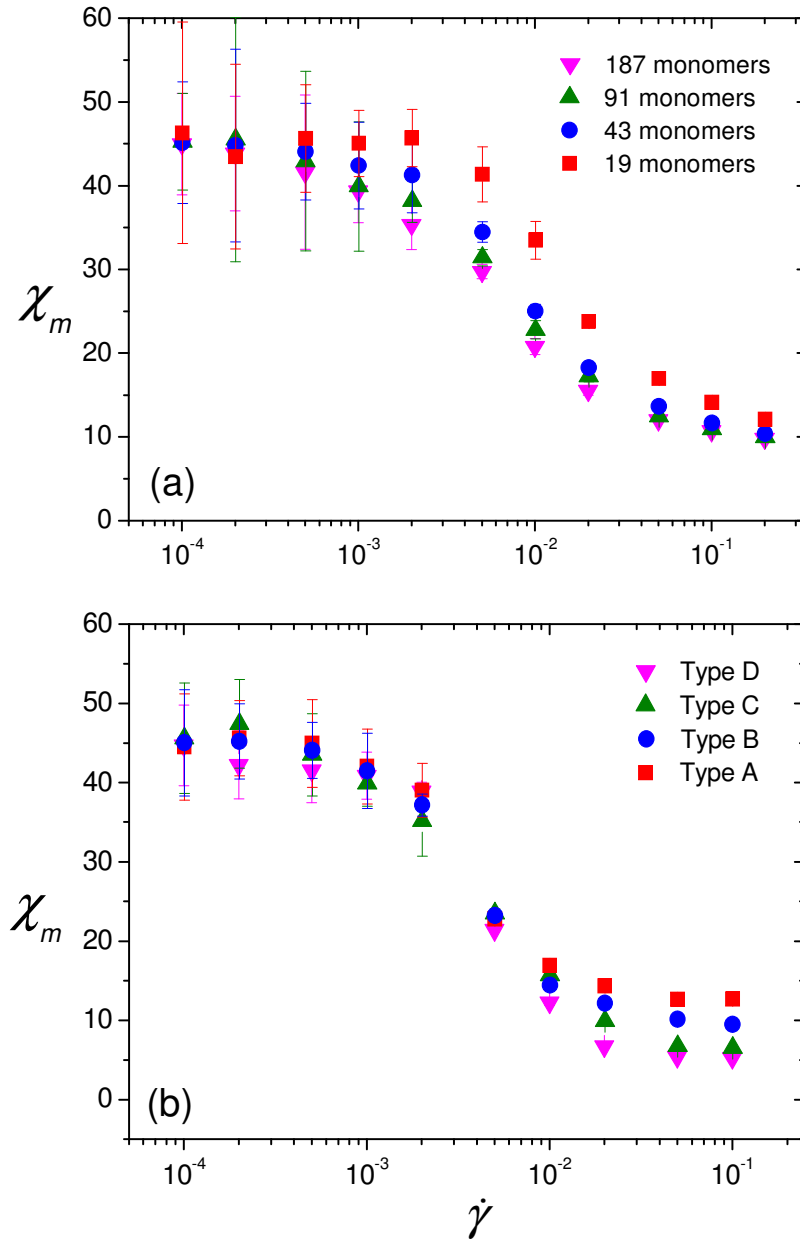
#### **5.8.1. Form birefringence**

In order to characterise the flow induced molecular alignment of hyperbranched polymers, the molecular order tensor  $\mathbf{S}_m$  has been computed as:

$$\mathbf{S}_m = \sum_{i=1}^N \left\langle \mathbf{u}_i \mathbf{u}_i - \frac{1}{3} \mathbf{I} \right\rangle \quad (5.10)$$

where  $\mathbf{u}_i$  is the unit vector denoting the orientation of the single molecules and  $N$  is the total number of molecules in the system. The direction in which molecules are aligned is indicated by the eigenvectors of the order tensor. The eigenvector corresponding to

the largest eigenvalue of the tensor of gyration denotes the orientation of the molecule  $\mathbf{u}_i$  and the birefringence extinction angle is the angle between the flow direction and the molecular alignment direction.



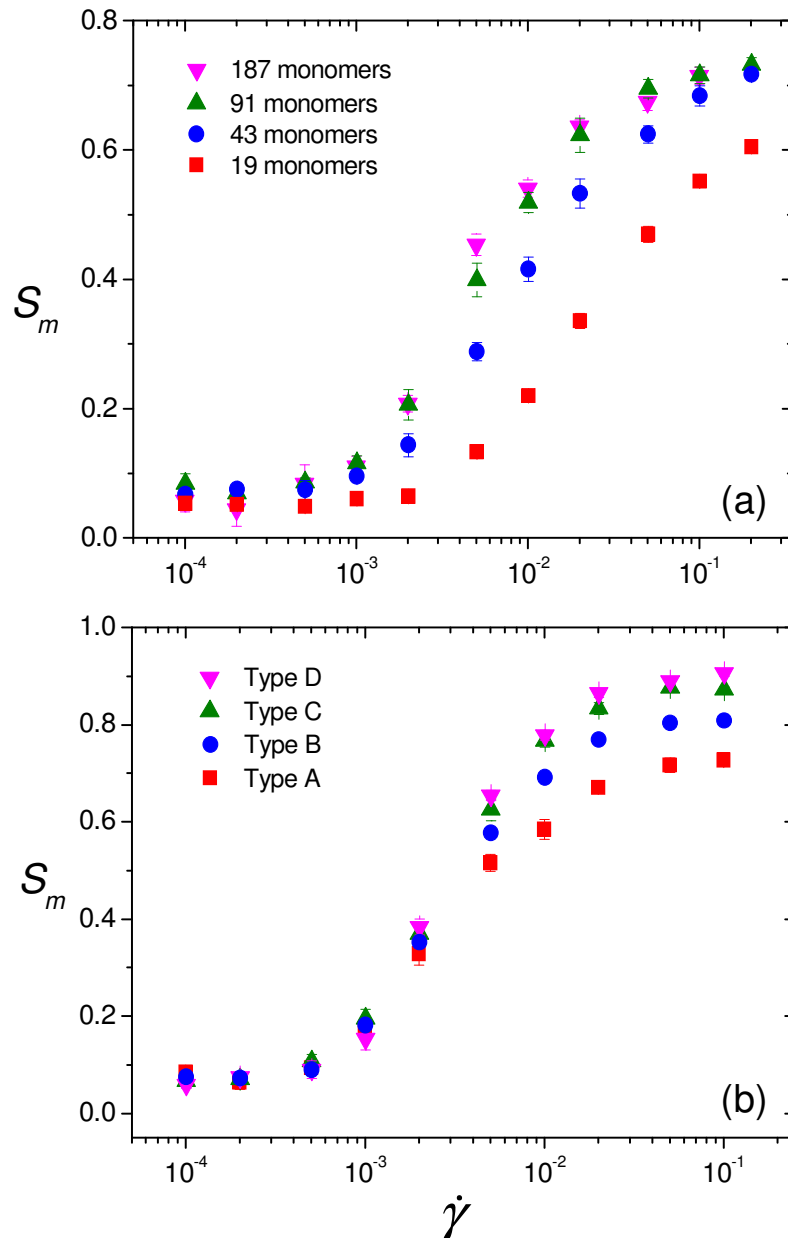
**Figure 5.28. Molecular alignment angle for hyperbranched polymers of (a) type A with different molecular weights and (b) the same molecular weight of 187 beads but different numbers of spacers.**

Figure 5.28 shows the molecular alignment angle which is the average angle between the flow direction and the molecular alignment direction for hyperbranched polymers of different molecular weights and different numbers of spacers. It can be seen that all

simulated systems reach the Newtonian region with the alignment angle of  $45^\circ$  in the range of considered strain rates. The  $45^\circ$  angle is expected for systems in the Newtonian regime due to the non-uniform spin angular velocity of molecular rotation in shear flow (Doi and Edwards, 1986). Furthermore Figure 5.28(a) shows that the alignment angle of large hyperbranched polymers departs from  $45^\circ$  at low strain rates whereas the alignment angle of small polymers remains close to  $45^\circ$  until higher strain rates are reached because these small polymers can rotate with the flow more easily. In comparison with other NEMD simulation data, our alignment angles in the non-Newtonian region are smaller than those for dendrimers and larger than those for linear polymers of the same molecular weight. This is because dendrimers have the most compact and constrained structure while hyperbranched polymers have less rigid architecture and linear polymers can stretch and align more easily with respect to the flow field, leading to anisotropic friction (Doi and Edwards, 1986). In Figure 5.28(b), it can be seen that at high strain rates where systems are in the non-Newtonian regime, hyperbranched polymers of type A have the highest values of the alignment angles  $\chi_m$  while polymers of type D have the lowest values of  $\chi_m$ . This again can be explained by the topologies of these systems. Type A hyperbranched polymers with the smallest number of spacers have the most compact and constrained structure. With increasing number of spacers, polymer architectures become less rigid, hence molecules and bonds can stretch and align more pronouncedly with respect to the flow field.

The order parameter  $S_m$ , which describes the extent of the molecular alignment, can be defined as  $3/2$  of the largest eigenvalue of the order tensor, which is a measure of the anisotropy of the average inertia tensor of a flexible molecule caused by the shear field (Doi and Edwards, 1986). This parameter equals 0 in the case of orientational disorder and reaches 1 for perfect alignment. Figure 5.29 presents the molecular order parameter of hyperbranched polymers with different molecular weights and different number of spacers. In all cases, the order parameter remains constant at low strain rates and rapidly increases in the high strain rate regions. This indicates that the orientational ordering increases and the alignment of the polymeric chains is more pronounced at higher strain rates. From Figure 5.29(a), it can also be seen that for any given strain rate, larger  $N$  polymer systems have larger values of  $S_m$  in comparison to smaller  $N$  polymer systems. However when the number of beads increases, the gap between the values of  $S_m$  for

hyperbranched polymers decreases. For the two largest systems of simulated hyperbranched polymers, the order parameter curves almost overlap. Furthermore, at the highest strain rate of 0.2, the order parameters for polymers comprising 43, 91 and 187 beads reach the same value of approximately 0.73.



**Figure 5.29.** Order parameter of the molecular alignment tensor for hyperbranched polymers of (a) type A with different molecular weights and (b) the same molecular weight of 187 beads but with different numbers of spacers.

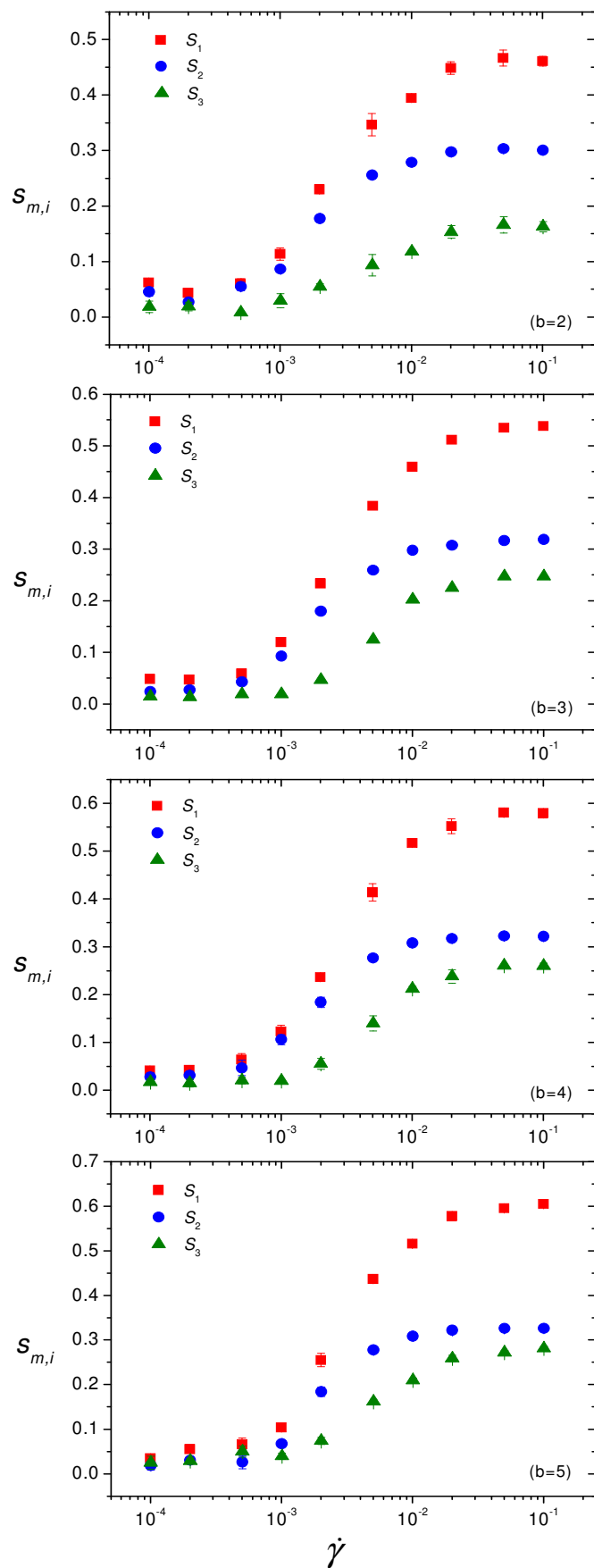


Figure 5.30. The eigenvalues of the molecular alignment tensor for hyperbranched polymers with the same molecular weight of 187 beads but different numbers of spacers.

Figure 5.30 presents the comparison of the eigenvalues of the molecular alignment tensor for hyperbranched polymers with different number of spacers. As can be seen, in all cases, the second and third eigenvalues are about half of the largest eigenvalues indicating weaker ordering in the other two directions. Such ordering is consistent with the prolate ellipsoid molecular shape characterized by the eigenvalues of the gyration tensor as discussed in the previous section.

### 5.8.2. Intrinsic birefringence

In order to characterize the intrinsic birefringence of hyperbranched polymer systems, the flow induced bond alignment has been analysed. The bond alignment tensor can be calculated as:

$$\mathbf{S}_b = \sum_j^N \left\langle \sum_{i=1}^{N_s-1} \mathbf{v}_i \mathbf{v}_i - \frac{1}{3} \mathbf{I} \right\rangle \quad (5.11)$$

where  $\langle \dots \rangle$  denotes an ensemble or time average and  $\mathbf{v}_i$  is the unit vector between neighbouring beads which can be defined as:

$$\mathbf{v}_i = \frac{\mathbf{r}_{i+1} - \mathbf{r}_i}{|\mathbf{r}_{i+1} - \mathbf{r}_i|}. \quad (5.12)$$

The flow alignment angle and the extent of the bond alignment can be calculated similarly to those of the molecular alignment in the previous section.

Figure 5.31 presents the bond alignment angle results for different hyperbranched polymers and linear polymers of equivalent molecular weight. As can be seen, the range of considered strain rates is wide enough for all hyperbranched polymer systems to reach the Newtonian regime where the bond alignment angle  $\chi_b$  is  $45^\circ$ . In contrast, for large linear polymers of 91 and 187 beads per molecule, the bond alignment angle cannot reach  $45^\circ$  in the considered range of strain rate. In order to reach the alignment angle of  $45^\circ$ , the systems would have to be simulated at lower strain rates. It can also be seen that in the non-Newtonian region, the bond alignment angle decreases with increasing strain rate. At a given strain rate, the bond alignment angle of larger molecules is smaller than that of the smaller ones. Our data for linear polymers are in good agreement with other NEMD simulation results (Kroger et al., 1993) which

indicated that the bond alignment of systems comprising no more than 60 beads can reach the Newtonian regime in the range of strain rates we have investigated.

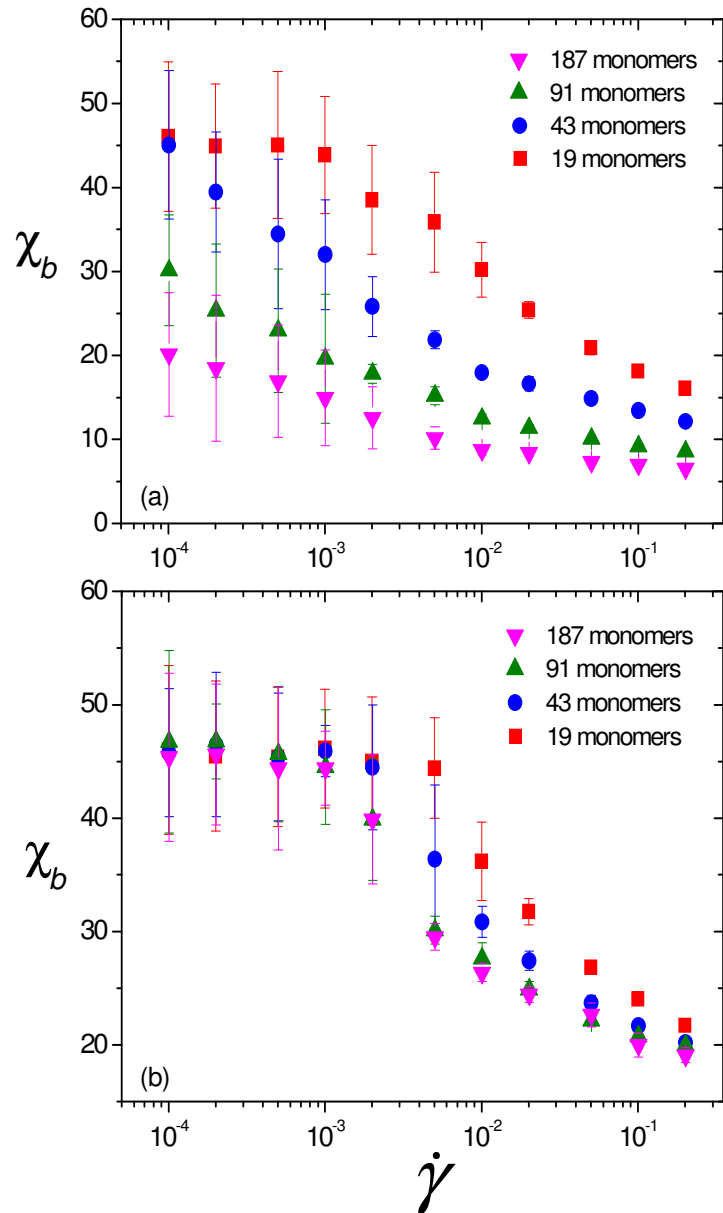
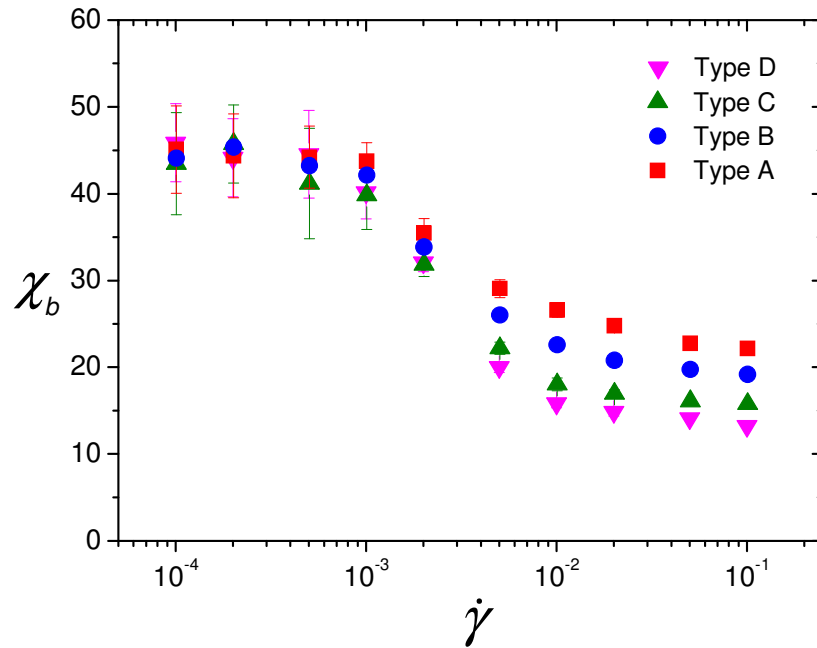
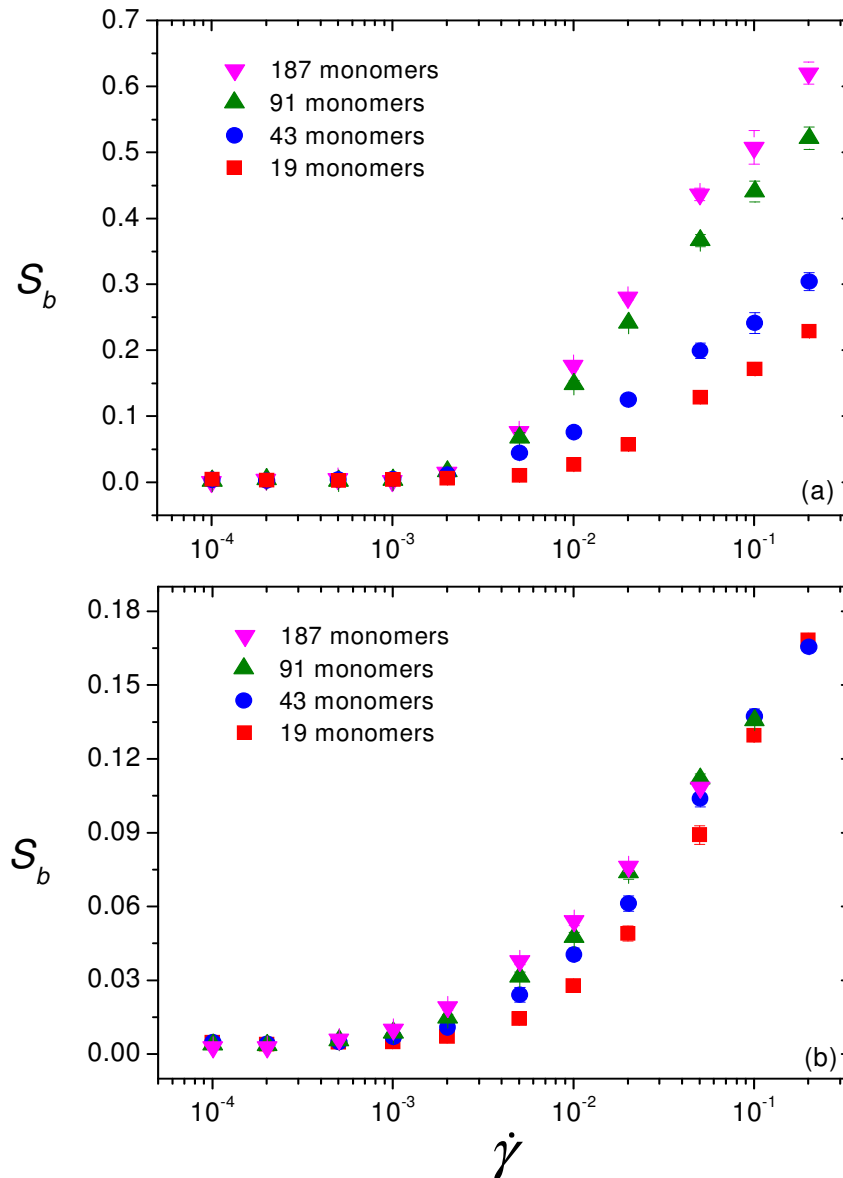


Figure 5.31. Bond alignment angle for (a) linear polymers and (b) type A hyperbranched polymers of different molecular weights.



**Figure 5.32. Bond alignment angle for hyperbranched polymers with the same molecular weight of 187 beads but different numbers of spacers.**

Figure 5.32 illustrates the bond alignment angle which is the angle between the flow direction and the bond alignment direction for hyperbranched polymers with different number of spacers. Similar to hyperbranched polymers of different molecular weights, at low strain rates where polymer systems are in the Newtonian regime, the bond alignment angles reach  $45^\circ$  and decrease at higher strain rates where systems are in the non-Newtonian regime. In comparison with the molecular alignment angle, at high strain rates, the bond alignment angle is always higher than the molecular alignment angle of the same polymer type. This is due to the packing constraints around branching points which prevent the simultaneous alignment of all bonds in the system, especially for the highly branched type A molecules.



**Figure 5.33. Bond order parameter for (a) linear polymers and (b) type A hyperbranched polymers of different molecular weights.**

Alignment in the shear plane can be characterised by the values of  $S_b$  which are shown in Figure 5.33.  $S_b$  is defined as 3/2 of the largest eigenvalue of the bond alignment tensor. These order parameters are a measure of the anisotropy of the average inertia tensor of flexible molecules or bonds caused by the shear field (Doi and Edwards, 1986). From Figure 5.33, it can be clearly seen that for both hyperbranched and linear polymer systems, all these values increase with increasing strain rates, and at the same strain rate, values for larger polymers are always higher than those for smaller polymers. This implies that for a given strain rate, the chain segments in large

molecules can more easily stretch and align with respect to the flow field. The  $S_b$  function of shear rate is monotonically increasing, but at high strain rates the values of  $S_b$  become the same for all hyperbranched polymer systems while those values are much higher for large linear polymers in comparison with small ones. Furthermore, at a given strain rate, the alignment parameter for hyperbranched polymers is always lower than that for linear polymers. This is because it is more difficult for hyperbranched chain segments to stretch and align with respect to the flow field as they have a more compact and constrained architecture. Our alignment results for linear polymers show good agreement with other NEMD simulation results (Kroger et al., 1993) although our data show slightly stronger alignment due to the difference in temperature and chain length of the systems.

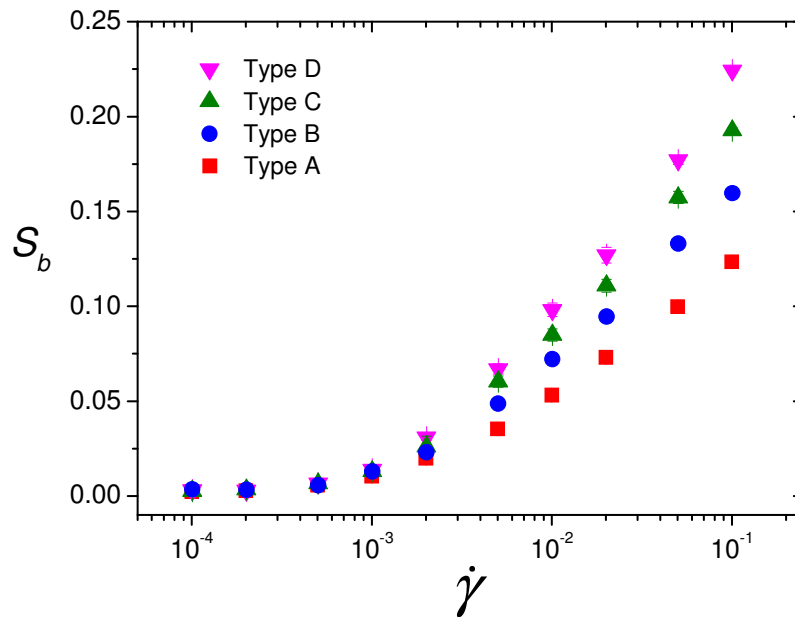


**Figure 5.34. Order parameter of the bond alignment tensors for hyperbranched polymers with the same molecular weight of 187 beads but different numbers of spacers at different strain rates.**

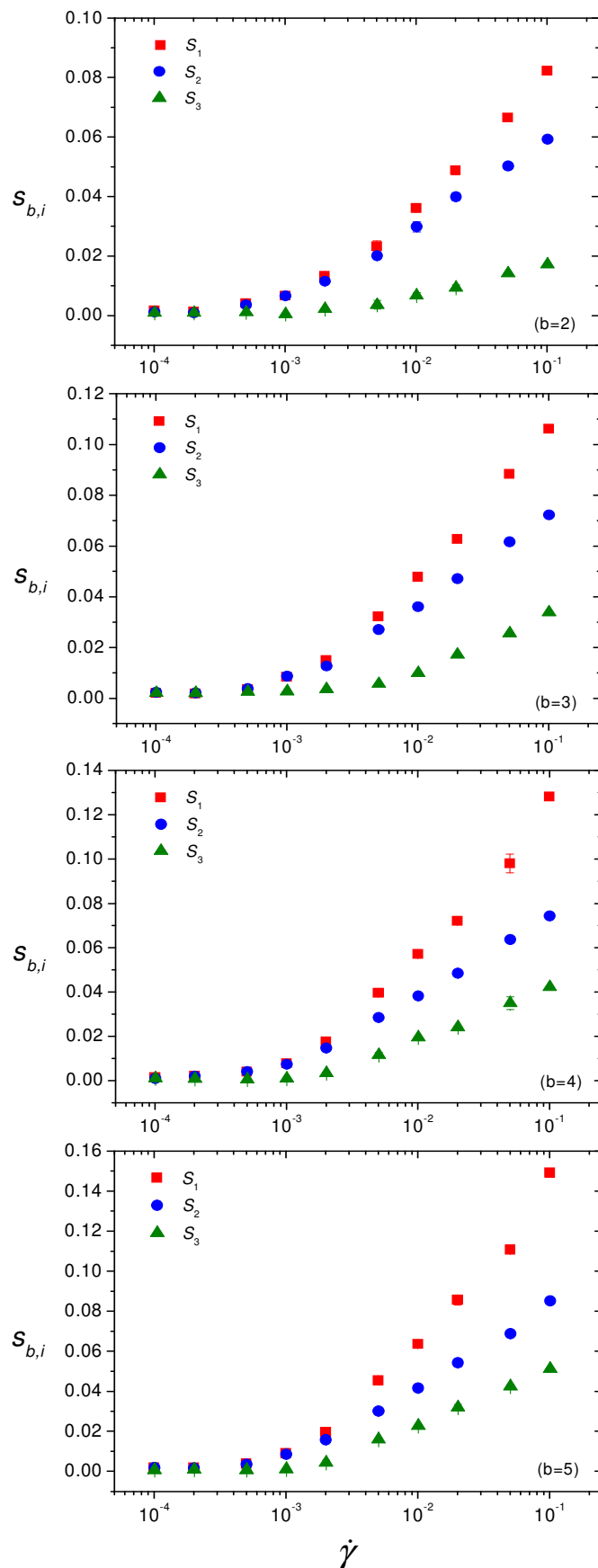


Figure 5.35. The eigenvalues of the bond alignment tensor for hyperbranched polymers with the same molecular weight of 187 beads but different numbers of spacers.

Figure 5.34 presents the bond order parameter  $S_b$  of hyperbranched polymers with different spacer lengths. Similar to the data for hyperbranched polymers of different molecular weights, in all cases, the order parameter remains constant at low strain rates and increases at high strain rates. This indicates that for all hyperbranched polymers, the orientational ordering increases and the alignment of bonds is more pronounced at high strain rates. It can also be seen that with increasing number of spacers, the order parameter increases. The alignment parameter for hyperbranched polymers with smaller number of spacers is always lower than that for polymers with larger number of spacers, because they have more compact and constrained structures and it is more difficult for the chain segments to stretch and align with respect to the flow field. Furthermore, in comparison to the molecular order parameter, the bond order parameter is always much lower due to the high level of branching of hyperbranched polymers and the excluded volume effect.

Figure 5.35 illustrates the comparison between eigenvalues of the bond alignment tensor for hyperbranched polymers with different spacer lengths. Similar to the case of the eigenvalues of the molecular alignment tensor, the second and third eigenvalues of the bond alignment tensor are only about half the magnitude of the largest eigenvalues. This shows that not only the molecular ordering but also the bond ordering in the other two directions is less pronounced.